JOURNAL OF GEOPHYSICAL RESEARCH, VOL. 115, D02112, doi:10.1029/2009JD012049, 2010

Interannual changes in mass consistent energy budgets from ERA-Interim and satellite data

Gabriel Chiodo[1,2] and Leopold Haimberger[1]

Received 12 March 2009; revised 16 September 2009; accepted 6 October 2009; published 28 January 2010.

[1] Diagnostic comparisons and evaluations of the global atmospheric energy and water budgets have been carried out with the new ERA-Interim reanalysis product and with satellite-derived fluxes. In the first part of this paper, we address time discretization, mass imbalance, and spin-up effects, which affect diagnostics from analysis and forecast fields in reanalysis. We discuss two ways of calculating vertically integrated horizontal energy and moisture flux divergence: (1) direct computation using analyzed fields and (2) indirectly from forecast model fluxes and vertically integrated tendencies. The spatial divergence patterns from the indirect method are found to be more realistic than those from direct computation from 6-hourly analyses since they are much less affected by temporal sampling errors, but corrections were nevertheless necessary to ensure mass consistency. The second part of this paper is focused on the interannual variability of ERA-Interim vertical fluxes and on comparisons with satellite flux data. Time series of vertically integrated energy/moisture tendencies and the corresponding analysis increments are also investigated, since shifts in these important quantities indicate artificial jumps in ERA-Interim, and relationships with vertical fluxes indicate internal consistency of the budgets. All data agree in that the most prominent changes in global budgets are internally forced (El Niño–Southern Oscillation). Broad agreement is found in ERA-Interim and Hamburg ocean atmosphere parameters and fluxes from satellite data (HOAPS-3) on a trend in the surface turbulent energy fluxes. Some of this trend may be caused by artificial shifts in ERA-Interim and especially HOAPS-3 in 1992 and possibly 2007. A strong increase in tropical land precipitation during the past decade is found in ERA-Interim and Global Precipitation Climatology Project 2. While large improvements have been made in terms of temporal homogeneity compared with ERA-40, especially with regard to precipitation, the homogeneity issue still needs to be carefully addressed when interpreting surface flux data from reanalyses or other sources.

Citation: Chiodo, G., and L. Haimberger (2010), Interannual changes in mass consistent energy budgets from ERA-Interim and satellite data, *J. Geophys. Res.*, *115*, D02112, doi:10.1029/2009JD012049.

1. Introduction

[2] The energy cycle is fundamentally dynamic. It is based on the conversion of incoming radiant into internal, potential, kinetic, and latent energy, moved around in various ways by the atmosphere and oceans, stored to a great extent in the ocean, and ultimatively radiated back to space [*Trenberth and Stepaniak*, 2004]. Certain mechanisms force the climate by altering the global energy balance, causing it to change, in order to reach a new "equilibrium." There are a number of mechanisms that can upset the energy balance over different time scales, such as, for instance, fluctuations in the Earth's orbit, volcanic eruptions, and changes in the ocean circulation and in the composition of the Earth's atmosphere. Changes in any of the climate system components, whether through internal or external forcings, cause the climate to vary or change. Water is present in three different phases in the climate system: gaseous (water vapor), solid (ice and cloud ice), and liquid (oceans, rivers, lakes, cloud water, and droplets). The hydrological cycle, through evaporative cooling and latent heating of the atmosphere, is intimately linked to the energy cycle.

[3] A precise knowledge of the energy and water fluxes on the Earth's surface and of horizontal transports in the atmosphere is essential in understanding the formation of the present climate as well as the processes of climatic changes in the past and the future. Accurate budget evaluations have been made possible in recent decades by the improvement of the global observational network. However, only satellites yield observations with high spatiotemporal resolution and global coverage. From 1978 onward, satellite observations became an increasingly important data source

[1]Department for Meteorology and Geophysics, University of Vienna, Vienna, Austria.
[2]Now at Departamento de Fisica de la Tierra, Astronomia y Astrofisica II, Facultad de Ciencias Fisicas, Universidad Complutense de Madrid, Madrid, Spain.

0148-0227/10/2009JD012049$09.00

for climate monitoring [*Climate Change Science Program*, 2006].

[4] Accurate computations of the vertically integrated budgets over a few years have been performed by several authors [*Trenberth*, 1997; *Trenberth et al.*, 2001, 2002a, 2002b; *Trenberth and Smith*, 2009; *Haimberger*, 2006] using improved data from reanalysis and satellite-derived products and quantifying the consistency of different data sets [*Yu et al.*, 1999]. These budget evaluations were also extended to coupled atmosphere-ocean systems [*Hantel*, 2005; *Trenberth and Caron*, 2001; *Trenberth and Stepaniak*, 2004]. Despite better input data, especially the energy budgets in these papers still appear relatively noisy, because horizontal energy flux divergences from routine analyses or from reanalyses are generally affected by time discretization errors, which are introduced by the coarse sampling in global analysis [*Haimberger et al.*, 2001]. Spurious mass flux divergences can also have detrimental effects on the energy budgets if they are not carefully dealt with. In this study we show that it is more accurate to calculate the horizontal divergences indirectly from the difference between short-term (12 h) forecast tendencies and forecast vertical fluxes.

[5] The studies noted earlier all consider time intervals that are too short to catch the interannual variability [*Haimberger*, 2006]. Availability of ERA-Interim data [*Simmons et al.*, 2006] now allows the depiction of interannual variability of the global atmospheric energy and moisture budgets, especially in the tropics, during the past 2 decades (1989–2008).

[6] In the second part, we focus on interannual variability and more on vertical flux divergences rather than horizontal flux divergences, which have to be zero in the long-term global mean. In this context, it is essential to compare our results from ERA-Interim with fluxes from International Satellite Cloud Climatology Project (ISCCP), Hamburg ocean atmosphere parameters and fluxes from satellite data (HOAPS-3), and Global Precipitation Climatology Project (GPCP-2) to assess inherent uncertainties. It is well known that changes in the observing systems used for deriving the earlier data sets may produce spurious trends and inhomogeneities, thus undermining the reliability of reanalysis data for long-term budget evaluations.

[7] It is crucial to assess the nature of shifts and trends in diagnostic evaluations, i.e., if they are artificial or true natural climatic fluctuations. During the period presented here, warm El Niño–Southern Oscillation (ENSO) events (1997) and volcanic eruptions (Pinatubo, 1991) leave clear signatures in the global energy and water cycle. On the other hand, some jumps and shifts may stem from satellite platform switches. We derive some internal diagnostics from ERA-Interim data, such as time series of vertically integrated analysis increments, that give valuable hints whether the shifts found in some ERA-Interim fluxes are artificial or natural.

[8] Section 2 outlines the data platforms used and the computational requirements. Section 3 highlights the theoretical background of the diagnostic budget evaluations. Two different methods to estimate transport divergences are discussed in section 4, along with mass imbalances, spin-up issues, and development of corrections in reanalysis forecast. Section 5 outlines the results of the long-term budget evaluations, including a comparison with satellite data and ECHAM5 simulations and assessment of internal consistency in global budgets. Section 6 summarizes the conclusions, highlighting the progress made in current research and the future strategies.

2. Data

[9] The ERA-Interim reanalysis is the main data source used for all energy and water budget evaluations in this work. Major improvements compared with previous reanalysis on temporal homogeneity and physical consistency have been achieved for ERA-Interim through variational correction of radiance biases and balanced parameterization schemes [*Simmons et al.*, 2006]. Twelve-hour forecasts and analysis of state variables (temperature, wind, and humidity) at full spatial resolution (T255, 60 vertical hybrid model levels) are used in this paper to obtain the best accuracy possible for the vertical integrals. The ERA-Interim surface fluxes are accumulated radiative and subgridscale heat fluxes from 12 h model forecasts. We also use ERA-40 data [*Uppala et al.*, 2005], the previous version of reanalysis, and compare some diagnostics that illustrate the progress made in ERA-Interim. The main advances in the ERA-Interim comprise 12 h four-dimensional variational analysis (4D-Var), variational bias correction of satellite radiance data, and improved model physics.

[10] Each energy and water budget component can be calculated with data sets from different sources. Satellite-derived fluxes are used to carry out a comparison with ERA-Interim, in the same way as several authors did in the past [e.g., *Trenberth*, 1997; *Trenberth et al.*, 2001]. Among all available satellite-derived data sets, we use ISCCP–flux data (FD) data covering the time period from July 1983 through December 2004 [*Zhang et al.*, 2004] for the radiation budget at top of the atmosphere (TOA), HOAPS for the surface sensible and latent heat fluxes, and GPCP precipitation data.

[11] The HOAPS data are a collection of global fields of air-sea interaction parameters such as sea surface temperature (SST), specific humidity, wind speed, evaporation, and other flux densities over the ice-free ocean [*Jost et al.*, 2002]. The latest released HOAPS version 3 contains all data ranging from 1987 to 2005. All variables are derived in this version from a combination of passive microwave measurements from the Special Sensor Microwave/Imager (SSM/I) with infrared imagery from the NODC/RSMAS Pathfinder SST V5 AVHRR for SSTs. In all budget evaluations, latent and sensible heat fluxes are used, as well as parameters such as evaporation and precipitation.

[12] We use data from the GPCP for the global precipitation distribution. The combination of rain gauge data with microwave and infrared estimates on the basis of SSM/I and TIROS operational vertical sounder (TOVS) makes this product superior to other precipitation data sets in terms of temporal and spatial homogeneity, particularly over land [*Adler et al.*, 2003]. The recently released GPCP version 2 covers the period January 1979 through present.

[13] Our diagnostics are also compared with ECHAM5 simulations, which were published by *Randall et al.* [2007]. More specifically, we chose uncoupled and coupled ECHAM5 simulations which were forced with observed and dynamic SSTs, respectively. These climate model simulations are

used to assess the effect of the SST forcing and of volcanic forcing on the water and energy budgets computed from data closer to observations (e.g., ERA-Interim and HOAPS).

3. Evaluation of Vertically Integrated Budgets

[14] Following *Trenberth* [1991], the vertically integrated moisture equation is considered as

$$\frac{\partial w}{\partial t} + \frac{1}{g}\int_0^{p_s} \nabla_2 \cdot q\mathbf{V}_2 \mathrm{d}p + P - E = 0, \quad (1)$$

where w is the precipitable water ($w = 1/g\int_0^{p_s} q\mathrm{d}\,p$), p_s is the surface pressure, q is the specific humidity, $\mathbf{V}_2$ is the horizontal wind vector, g is the gravitational acceleration, and E (positive upward) and P (positive downward) represent surface evaporation and precipitation. The second term is the vertically integrated horizontal moisture flux divergence. ∇_2 is the horizontal nabla operator. Physical units for all quantities in the aforementioned equation are mass flux density units (kg m^{-2} s^{-1}). Multiplying by the latent heat L gives energy flux units (W m^{-2}). (An empirical function of temperature for the latent heat L is taken from IFS documentation [*European Centre for Medium-Range Weather Forecasts*, 2006].)

[15] The vertically integrated total energy equation reads as

$$\frac{\partial}{\partial t}\frac{1}{g}\int_0^{p_s}\left(c_pT + k + Lq + \Phi_s\right)\mathrm{d}p + \frac{1}{g}\int_0^{p_s}\nabla_2\cdot(h+k)\mathbf{V}_2\mathrm{d}p + F_s - \mathrm{Rad}_{\mathrm{TOA}} = 0, \quad (2)$$

with

$$F_s = \mathrm{LH} + \mathrm{SH} + \mathrm{Rad}_S, \quad (3)$$

where F_s is the net surface energy flux, composed of LH, SH, and Rad_S, which are the subgrid-scale latent and sensible heat fluxes and net surface radiation, respectively; c_p is the specific heat at constant pressure; and Φ_s is the surface geopotential. $\mathrm{Rad}_{\mathrm{TOA}}$ is the net radiation at the top of the atmosphere, and $h = c_pT + \Phi + Lq$ is the moist static energy. Note that all fluxes are positive downward. The first term in equation (2) is the rate of the atmospheric storage of internal, potential, kinetic, and latent energy, which is in sum the total energy e. Throughout this paper, we will refer to this term as the atmospheric storage rate.

[16] In short form, we write

$$\frac{\partial\langle e\rangle}{\partial t} + \langle\nabla_2\cdot F_a\rangle + F_s - \mathrm{Rad}_{\mathrm{TOA}} = 0, \quad (4)$$

where the $\langle\rangle$ operator denotes the vertical integral $g^{-1}\int \mathrm{d}p$, F_a is the horizontal energy flux; therefore, $\langle\nabla_2 F_a\rangle$ is the vertically integrated horizontal energy flux divergence. The difference ($F_s - \mathrm{Rad}_{\mathrm{TOA}}$) represents the vertical energy flux divergence in an atmospheric column, also defined as the vertically integrated atmospheric diabatic heating rate in many of Trenberth's publications [e.g., *Trenberth and Stepaniak*, 2004]. In terms of absolute values, the vertically integrated horizontal energy flux divergence is dominated by the moist static energy flux divergence ($\langle\nabla_2 hV\rangle$) (about 10^9 J m^{-2}), while the integrated kinetic energy flux divergence ($\langle\nabla_2 kV\rangle$) is smaller by a factor of 10 but not negligible [*Trenberth et al.*, 2002a].

[17] Equation (2) states that the change of energy in an atmospheric column is the net result of the exchanges of energy with the surrounding columns, outer space, and the underlying surface [*Peixoto and Oort*, 1992]. The atmospheric energy and water budgets are locally dominated by the vertically integrated atmospheric lateral energy and moisture transport (second term on left-hand side of equations (1) and (2)) and the net vertical fluxes ($F_s - \mathrm{Rad}_{\mathrm{TOA}}$ and P-E), while the atmospheric rate of storage and precipitable water are relatively small (first term in the left-hand sides) on seasonal to annual time scales.

[18] Neglecting the storage rates on annual time scales and further separating land and ocean columns, the energy and water budget equations thus reduce to a balance between transport divergences and net vertical fluxes (second, third, and fourth terms in equations (1) and (2)). Further simplifications are possible over land, where annual mean surface energy fluxes F_s vanish and so the TOA radiation must balance the vertically integrated horizontal energy divergence (equation (5)). Over the ocean, F_s is nonzero and is the driving force for lateral energy fluxes within the oceans (equation (6)). Hence, the vertically integrated horizontal energy flux divergence must balance the term in the right-hand side ($\mathrm{Rad}_{\mathrm{TOA}} - F_s$).

$$\left\langle\nabla_2\cdot F_a^{\mathrm{land}}\right\rangle = \mathrm{Rad}_{\mathrm{TOA}} \quad (5)$$

$$\left\langle\nabla_2\cdot F_a^{\mathrm{ocean}}\right\rangle = \mathrm{Rad}_{\mathrm{TOA}} - F_s. \quad (6)$$

These simplifications can be used to put physical constraints on the global energy budget evaluations in section 4.

4. A New Method to Estimate the Horizonal Transport Divergence and Energy Storage

[19] Global water and energy budgets can be calculated from ERA-Interim in various ways. The third and fourth terms in the left-hand sides of equations (1) and (2) are obtained from accumulated subgrid-scale nonadvective (LH + SH and P-E) and radiative ($\mathrm{Rad}_{\mathrm{TOA}}$ and Rad_S) fluxes through 12 h integrations of the European Centre for Medium-Range Weather Forecasts (ECMWF), Reading, UK, operational atmospheric forecast model. There are two possible methods to estimate the horizontal energy and moisture transport divergence, i.e., the second terms in equations (2) and (1). One is through direct computation, and the second is through indirect inference by calculating these terms as residuals from the other budget terms.

[20] The direct method requires a mass consistent wind field, i.e., the wind data must fulfil the discretized continuity equation. Consistency is often enforced through diagnostic mass flux modification schemes [*Trenberth*, 1991, 1997; *Trenberth and Guillemot*, 1995; *Trenberth et al.*, 2001, 2002a; *Haimberger*, 2006]. Such a mass flux modification is necessary even when using ERA-Interim data on the original vertical hybrid model levels [*Haimberger*, 2006]

since the mean surface pressure tendency inferred from the vertically integrated divergence of the analyzed wind in the continuity equation is nonzero on long time scales. This tendency is spurious and must be adjusted to zero for long-term means or to the analyzed surface pressure tendency at shorter time scales. The effect of the adjustment can be illustrated by considering the vertically integrated horizontal total energy flux divergence. It can be divided into two terms as

$$\frac{1}{g}\int_0^{p_s} \nabla\cdot(h+k)\mathbf{V}_2 \mathrm{d}p \approx \left(\widehat{h}+\widehat{k}\right)\frac{1}{g}\frac{\partial p_s}{\partial t}+\frac{1}{g}\int_0^{p_s}\mathbf{V}_2\nabla\cdot(h+k)\mathrm{d}p \tag{7}$$

where circumflex denotes the vertical average on hybrid model levels and p_s is the surface pressure. The first term in the right-hand side of equation (7) represents the contribution of mass flux divergences to the energy transport divergence. The relationship is not exact because the vertical correlation between $h + k$ and $\nabla\vec{v}$ has been neglected. Since $h + k$ generally shows little variation in the vertical in the troposphere, this approximation seems adequate. The surface pressure tendency needs to be corrected to match the analyzed surface pressure tendency before the horizontal energy and moisture flux divergences are computed. Direct estimates in Figures 5 and 6 have been calculated in this way.

[21] Even after this mass flux correction, the estimated energy flux divergence can still have systematic errors on the order of 20% [*Haimberger et al.*, 2001] because of large temporal sampling errors due to the coarse time resolution of global analysis (6 h in ERA-Interim and ERA-40). The temporal sampling problem in the direct method could only be circumvented if the divergences were accumulated during the first hours of the model runs, as is done with surface fluxes. Unfortunately, this has not been done routinely in any reanalysis so far because of storage space considerations.

[22] The temporal sampling problem can be circumvented, however, at least for vertical integrals, if the vertically integrated horizontal energy divergence is estimated indirectly as a residual from forecast vertical fluxes (F_s and $\mathrm{Rad_{TOA}}$) and fields of the forecast local tendency ($(\partial/\partial t)w$ and $(\partial/\partial t)\ \langle e\rangle$ in equations (1) and (2)). The "indirect" method involves a better sampling (the typical model integration step to calculate vertical fluxes and forecast fields amounts to approximately 15 min). One may argue that the indirectly estimated horizontal divergences are mean forecast divergences from forecast hours 0 to 12 and no longer analyzed divergences. The indirect method also creates a formal dependence for the horizontal divergences on the model parameterizations of physical processes, which influence radiation and subgrid-scale fluxes (F_s and $\mathrm{Rad_{TOA}}$) and forecast tendencies. As we will show in the following, however, this dependence on the forecast model is not stronger than it is for the directly estimated flux divergences. Moreover, the indirect estimates are less noisy.

[23] Even for the indirect approach, we need accurate computation of local tendency terms in equations (1) and (2). For the tendencies, there is no time sampling problem, as the atmospheric rate of storage reduces to a simple difference between the energy content at the end and at the beginning of the considered time interval. Like the horizontal divergences, the forecast tendencies can also be affected by mass inconsistencies, which can be removed, however. Following the Leibniz rule of integration, the storage rate term can be broken down into two terms:

$$\frac{1}{g}\frac{\partial}{\partial t}\int_0^{p_s(t)} e\mathrm{d}p = \frac{1}{g}\int_0^{p_s(t)}\frac{\partial e}{\partial t}\mathrm{d}p + \frac{e(p_s)}{g}\frac{\partial p_s}{\partial t}. \tag{8}$$

[24] The contribution of the local energy tendency to the total atmospheric storage rate is given from the first term in the right-hand side of equation (8), while the second one is the energy change through the surface pressure tendency. A change in surface pressure can be obtained through mass displacements (horizontal mass convergence/divergence). Accordingly, the energy content of an atmospheric column can increase (decrease) through a mass-specific energy increase (decrease) and/or through mass transport convergence (divergence). We will consider both the analyzed and the 12 h forecast energy tendencies in the following.

[25] Figure 1 shows the atmospheric rate of energy storage (first term in the left-hand side of equation (2) and left-hand side of equation (8)) in ERA-Interim for January 1990. When averaging over 1 month, the analyzed 12 h tendencies reduce to the difference between the last and the first day of the considered month: January 1990. The signature of synoptic activity is dominant in midlatitudes and explains most of the spatial structures. It must be reminded that if using analysis, this budget term vanishes in the long term.

[26] A separate computation of the two terms in the right-hand side of equation (8) reveals that the energy change patterns seen in Figure 1 are mostly explained through mass transport divergence/convergence (second term in the left-hand side of equation (8)). Thus, it can be stated that the variability of the atmospheric rate of energy storage is dominated on monthly time scales by the surface pressure tendency term in equation (8), which accounts for about 70%–75% of the total rate of energy storage. (The energy at the surface is a monthly average, while the pressure tendency is the difference between the mean pressure on the last day and the first day of the month.)

[27] To be consistent with the indirect approach of inferring the horizontal energy divergence from 12 h forecasts of vertical subgrid-scale fluxes F_s and $\mathrm{Rad_{TOA}}$ in equation (2), the storage rate term needs to be calculated by averaging 12-hourly forecast tendencies. Hence, the storage rate term does not reduce to a simple difference between the energy content at the end and at the beginning of the considered time interval.

[28] Figure 2 shows the estimates of this term from differences between 12 h model forecasts and analysis in ERA-Interim. There is ample evidence of biased tendencies throughout the tropics and the subtropics at 45°E–90°E. The same pattern is replicated with 6 h data (not shown), which clearly rules out the influence of semidiurnal tides aliasing [*Trenberth*, 1991].

[29] Such structures in the forecasts originate from systematic model errors, as the departure of the forecasts from the analysis is not randomly distributed over a month but has a nonzero mean for certain grid points instead. During

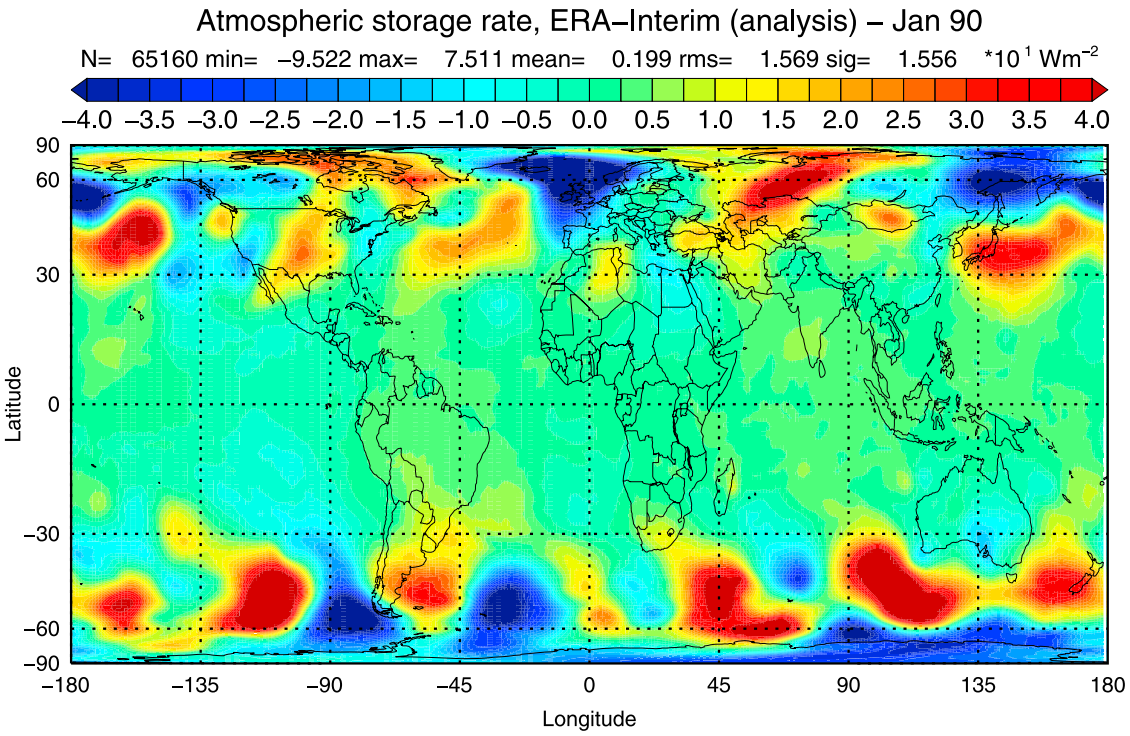

Figure 1. Average storage rate in January 1990 from ERA-Interim analysis fields at the end and at the beginning of the month (unit is W m^{-2}).

the assimilation cycle, the model tends to drift to its own climate, represented in the global mean by a lower atmospheric total energy content, at least in January 1990. The negative global mean (−4.04 W m^{-2}) in Figure 2 shows that the energy conservation constraint is not completely fulfilled with model forecasts within monthly time scales, as this value dwarfs the typical yearly cycle (±1 W m^{-2}) of the global mean atmospheric energy content [*Peixoto and Oort*, 1992].

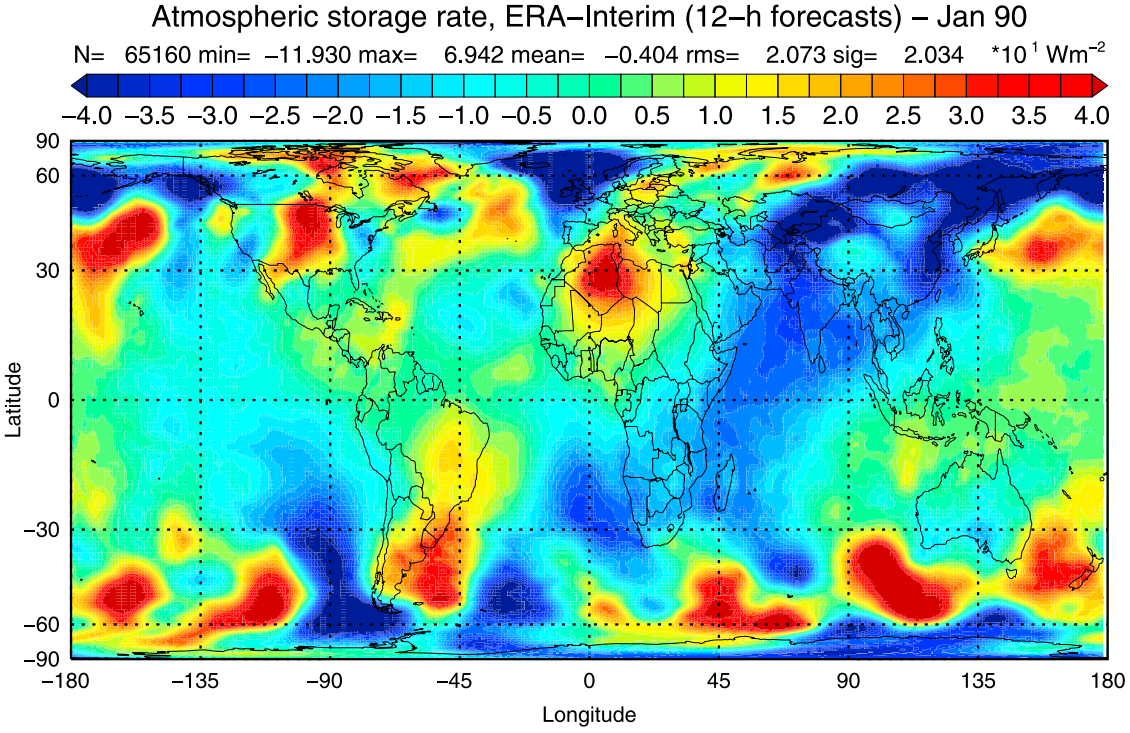

Figure 2. Mean total energy storage rate in January 1990 calculated from averaging 62 12 h forecast tendencies (unit is W m^{-2}).

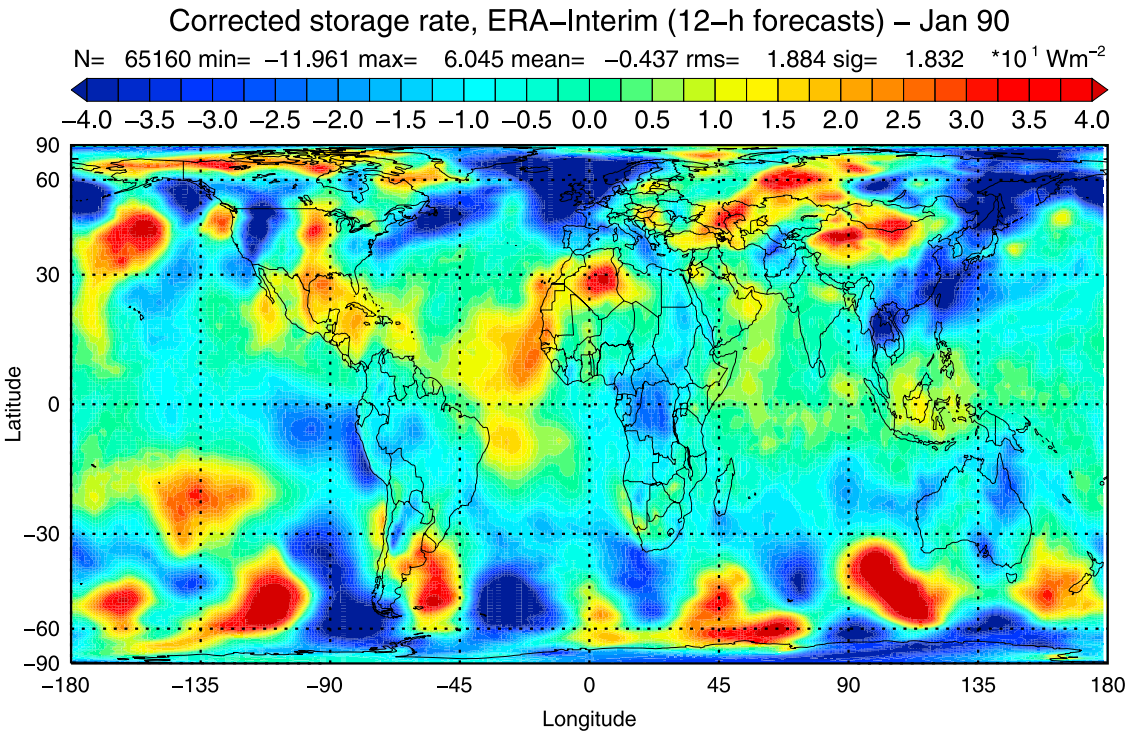

Figure 3. Same as Figure 2 after subtracting the spurious monthly mean forecast pressure tendency (second term in the right-hand side of equation (8)) (unit is W m^{-2}).

[30] We developed a weighted correction against wrong pressure tendencies in reanalysis to avoid such mass inconsistencies. As a first step, we estimated the erroneous forecast pressure tendencies as differences between 12 h forecast and analyzed surface pressure values. This difference is then multiplied by the total energy at the surface, following the definition of the second term in the right-hand side of equation (8). The mathematical definition of the mass flux corrected mean forecast atmospheric storage rate reads as follows:

$$\frac{\partial}{\partial t}\langle e^{\mathrm{fc}}\rangle^{*} = \frac{\partial}{\partial t}\langle e^{\mathrm{fc}}\rangle - \frac{\overline{e(p_{\mathrm{s}})}}{g}\frac{\partial}{\partial t}\left(p_{\mathrm{s}}^{\mathrm{fc}} - p_{\mathrm{s}}^{\mathrm{an}}\right) \tag{9}$$

where $\overline{e(p_{\mathrm{s}})}$ denotes the monthly mean of the total energy at the surface, "fc" means forecast, and "an" means analysis. The first term in the right-hand side is the original field computed with forecast and analysis fields, which corresponds to the term in the left-hand side of equation (8). The second term represents the applied correction for wrong pressure tendencies, as the difference between the analyzed ($p_{\mathrm{s}}^{\mathrm{an}}$) and forecast ($p_{\mathrm{s}}^{\mathrm{fc}}$) surface pressure is a bias measure (both are valid for the same time with a 12 h resolution). After applying the pressure correction, the spurious storage rate, e.g., over the Indian Ocean in the tropics, is removed (see Figure 3), but the spatial structures at higher latitudes of both hemispheres, containing (real) climatic signals of baroclinic activity, are not affected.

[31] For later reference, we also introduce an adjustment of the vertically integrated ERA-Interim total energy analysis increment. The analysis increment is the difference between the 12 h forecast energy content and the analyzed energy content. This difference again has a thermodynamic contribution and a mass contribution. We are only interested in the thermodynamic contribution. Therefore, we again subtract the surface pressure analysis increment ($p_{\mathrm{s}}^{\mathrm{fc}} - p_{\mathrm{s}}^{\mathrm{an}}$),

$$\frac{\partial}{\partial t}\langle e^{\mathrm{fc}} - e^{\mathrm{an}}\rangle^{*} = \frac{\partial}{\partial t}\left(\langle e^{\mathrm{fc}}\rangle - \langle e^{\mathrm{an}}\rangle\right) - \frac{\overline{e(p_{\mathrm{s}})}}{g}\frac{\partial}{\partial t}\left(p_{\mathrm{s}}^{\mathrm{fc}} - p_{\mathrm{s}}^{\mathrm{an}}\right). \tag{10}$$

[32] This pressure tendency adjusted diagnostic is very sensitive to imbalances between observations and the climate of the assimilating model. Hovmöller plots of this quantity are shown in section 5.

[33] If we now go back to analyzing the energy storage, we must see that despite the adjustment of the surface pressure tendency, there remains a global imbalance, as the global mean energy storage is still far from zero (−4.37 W m^{-2}), which indicates systematic cooling throughout the first 12 forecast hours. Yet another remarkable feature of the rate of storage term from corrected forecasts is that it contains many more structures and much more variability than if it is computed from analysis alone (the global RMS in the analysis and forecast-analysis field is 15 and 20 W m^{-2}), which is due to the contribution of high-frequency (12 h) variability.

[34] Even though realistic structures for the vertical energy flux divergence ($F_{\mathrm{s}} - \mathrm{Rad}_{\mathrm{TOA}}$) seem to be captured qualitatively well in January 1990, a global mean of 9.57 W m^{-2} (not shown) is unrealistic, since it exceeds by far the small yearly cycle due to the nonuniform ocean-land distribution in the two hemispheres [*Peixoto and Oort*, 1992]. A vertical energy flux divergence of this magnitude would translate to a global cooling of about 3 K/month in ERA-Interim. We looked for the origin of the bias by calculating global means of ERA-Interim TOA radiation and F_{s} and then

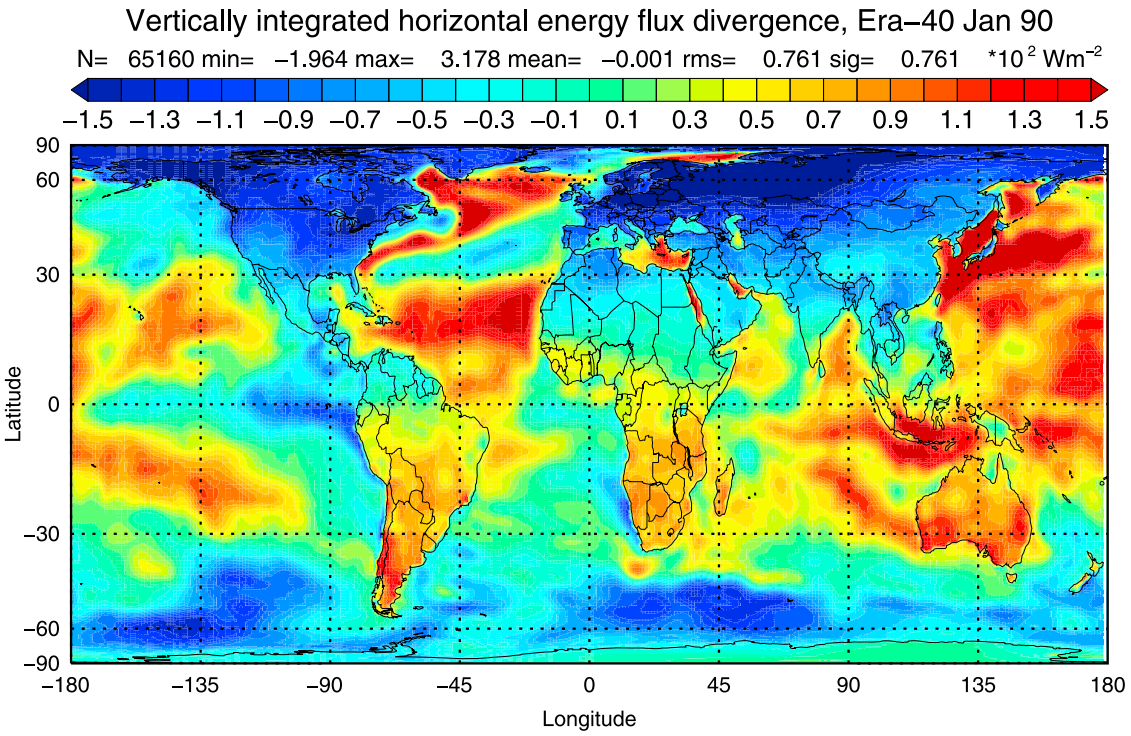

Figure 4. Vertically integrated horizontal energy flux divergence in January 1990, computed indirectly as a residual from adjusted forecast energy tendency and vertical energy flux divergence in ERA-40. Note that positive values denote divergent transports (unit is W m^{-2}).

comparing it with other satellite data sets like HOAPS-3 and ISCCP-FD. It is found that the radiation at TOA is balanced within 3–4 W m^{-2} in all data sets, while the global mean of the ERA-Interim surface energy fluxes (F_s) amounts to +15.4 W m^{-2} in this month, which means a global net energy flux into the surface. The combination of HOAPS-3 for the surface latent plus sensible heat fluxes (LH + SH) and ISCCP-FD data for TOA radiation would even amplify the overall imbalance; therefore, we chose to use exclusively ERA-Interim fluxes with an uniform adjustment to achieve a balance in global energy budgets.

[35] There is a clear evidence that the imbalance source is represented by the surface energy fluxes over the oceans, thus violating the consistency condition defined in equation (6). A longer (24 h) atmospheric model integration in ERA-Interim results in reduced net fluxes, but the extent of the decrease (1 W m^{-2} in the global mean) is still unsatisfactory. Nevertheless, this is an improvement compared to ERA-40, where *Trenberth and Smith* [2009] and *Haimberger* [2006] found imbalances having the same sign and bigger magnitudes. According to these results, the use of a correction for these imbalances is required before calculating any quantities as residuals. We adopt the common [*Zhang and Rossow*, 1997; *Trenberth et al.*, 2001; *Haimberger*, 2006] method consisting of a uniform adjustment represented by the global mean.

[36] After tuning the original data to correct (1) the spurious pressure tendency forecasts and (2) the model spin-up in surface energy fluxes, a balanced (global mean is zero) vertically integrated horizontal energy flux divergence can now be inferred for ERA-Interim data.

[37] For validation purposes, a comprehensive comparison between the indirect and the direct method is of high relevance. Unfortunately, this was only feasible for ERA-40 (see Figure 4), since this is the only ECMWF set of reanalysis for which the horizontal atmospheric energy divergence fields have been calculated directly and stored routinely, although only from the 6-hourly analysis data during postprocessing. No such postprocessing has been available for ERA-Interim so far.

[38] The direct estimates of the vertically integrated horizontal energy divergence from ERA-40 needed a correction against spurious mass flux divergence. This was done by subtracting the first term in the right-hand side of equation (7). Data with 6 h resolution were preferred, because 12-hourly data cannot resolve semidiurnal tides with acceptable accuracy [*Trenberth*, 1991]. Figure 5 shows the results for this budget computation on the basis of ERA-40. The isolated positive signals over land (e.g., Russia, Antartica, and Canada) are mostly spurious, as they would produce an imbalance with the TOA radiation, according to the consistency condition defined in equation (5). Signals over mountainous regions of over 100 W m^{-2} are related to errors in the divergence of potential energy, which stem from truncation errors and other numerical problems [see *Trenberth et al.*, 2002a].

[39] The indirect (Figure 4) and direct (Figure 5) estimates of the ERA-40 vertically integrated horizontal energy divergence show good large-scale agreement. The physical mechanism explaining such structures is a strong energy export by the Hadley equatorward branch at ~20°N and baroclinic eddies at ~50°N over the oceans in the Northern

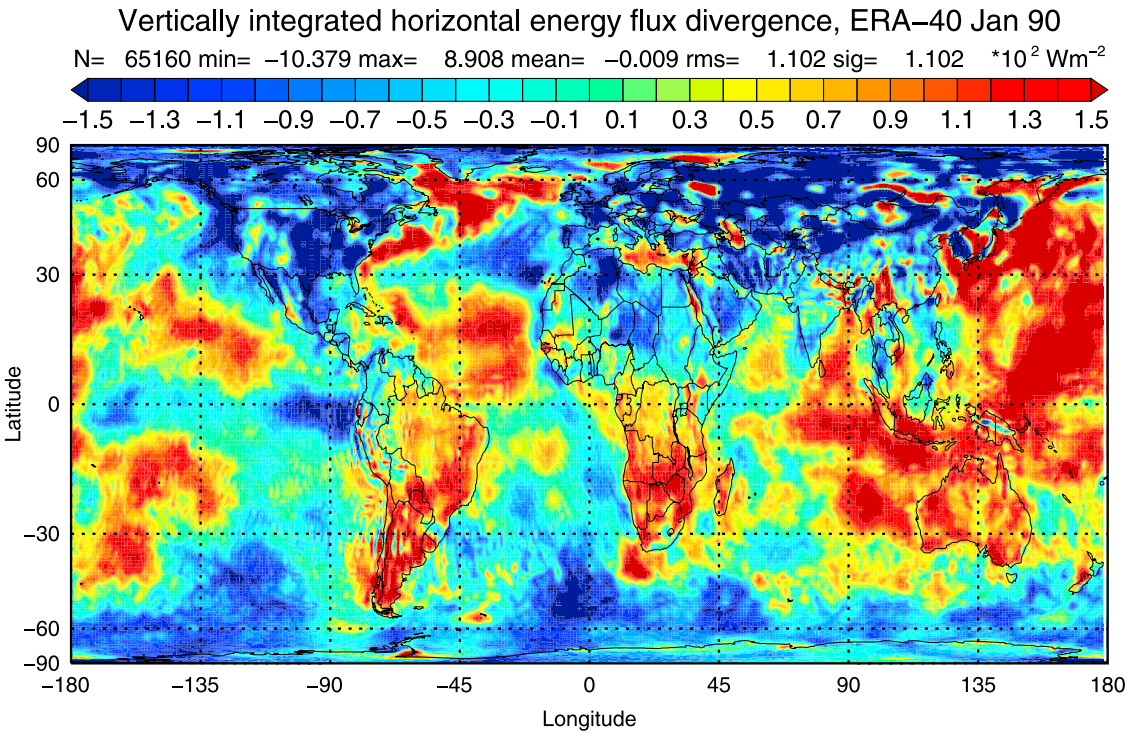

Figure 5. Direct estimate of the vertically integrated horizontal energy divergence in January 1990, as stored routinely in ERA-40 from 6 h wind, humidity, and temperature analysis. Divergence fields have been corrected against spurious mass flux divergence by subtracting the first term in the right-hand side of equation (7) (unit is W m^{-2}).

Hemisphere. Also, the divergence over land in the Southern Hemisphere is well replicated in both methods. However, quantitative discrepancies need further attention. The indirect method does not produce the large (over 100 W m^{-2}) land imbalances which affect the results obtained through the direct method in Figure 5. The global root-mean-square value drops from 110 W m^{-2} in the direct estimate (Figure 5) to 76 W m^{-2} in the indirect (Figure 4) inference method. Thus, the indirect estimate seems to give physically more reasonable results with much less noise. In the zonal mean, the indirect (blue line) and direct (dashed line) methods show acceptable agreement for ERA-40 (Figure 6), although differ-

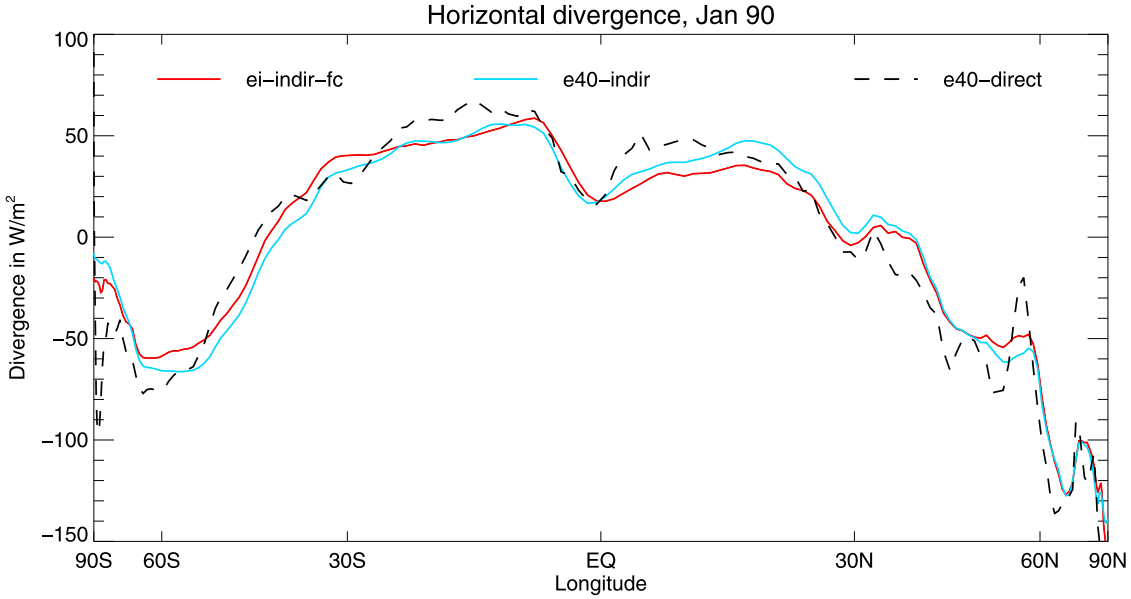

Figure 6. Zonal means of the vertically integrated horizontal energy flux divergence. The red line denotes the indirect estimate for ERA-Interim, the blue line is the indirect estimate for ERA-40, and the dashed black line is the direct estimate for ERA-40 (unit is W m^{-2}).

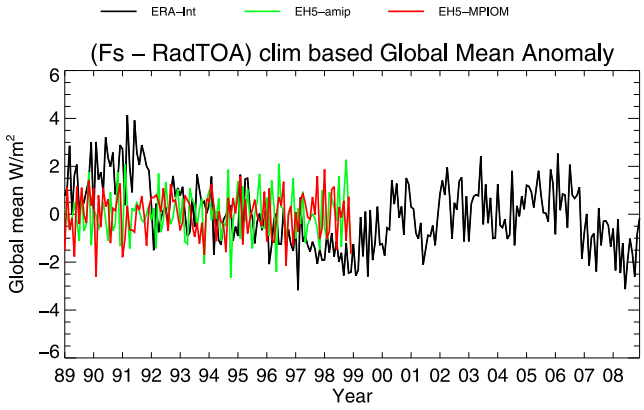

Figure 7. Anomaly of the global mean to long-term (1989–2008) climatology of the vertical energy flux divergence (F_s − Rad_{TOA}) (in W m^{-2}) for ERA-Interim, ECHAM5-AMIP (ocean-uncoupled ECHAM5 simulation forced with AMIP SSTs), and ECHAM5-MPIOM (ocean-coupled ECHAM5-mpiom simulation). Negative values denote net positive heating rate, which indicates warming of the atmospheric column. All fluxes are positive downward (unit is W m^{-2}).

ences amount to 20 W m^{-2} in the subtropics. The tropical minimum in the bimodal distribution is related to the compensation between the low-level moisture convergence that feeds the upward branch of the Hadley circulation and the net dry static energy divergence driven by the upper level poleward branch [*Trenberth and Stepaniak*, 2004]. The unrealistic peak at 60°N in the ERA-40 direct estimate is not found in the indirect method for both ERA-40 and ERA-Interim (red line), thus supporting the view of physically better results.

[40] The two methods have also been compared for the vertically integrated horizontal moisture divergence in equation (1). It is found that the indirect method yields the same (within ±1 W m^{-2}) horizontal moisture flux divergence values as the direct estimate (not shown). Both estimates are also equally sensitive to the assimilating model, as is shown by *Chiodo* [2008, Figure 4.14].

[41] We note here that the previous considerations are especially important for regional evaluations. The horizontal divergence is less important for time series of global and zonal means, which we shall show in section 5, since it has to be zero in the global mean.

5. Interannual Variations in the Energy and Water Budgets

[42] The ultimate purpose of our diagnostics is to investigate the interannual variations of the global energy and water budgets. Focus will be given to the period 1989–2008, although with special emphasis on the first decade (1989–1998), since it is covered by all data sets used here for comparisons with ERA-Interim. Detection of true interannual changes can only be achieved if data inconsistencies related to mass balance and time discretization are avoided by applying the correction methods that have been developed in section 4. However, when considering long time series, we have a new potential source of inconsistencies that we cannot avoid: changes in the observing system. We shall see that time series of analysis increments can give valuable hints in this respect. It is also quite interesting to compare budget evaluations from ERA-Interim and satellite data with an internally consistent model in which no observations are assimilated, so we included output from a Global Circulation Model (GCM) in our diagnostics. The ECHAM-5 climate modeling system was chosen because the dynamical core has been developed from the ECMWF operational forecast model [*Roeckner et al.*, 2003]. Two different ECHAM5 control run simulations were taken with the same resolution (T63L31): an uncoupled simulation experiment with observed AMIP sea surface temperatures and sea ice concentration climatology [*Roeckner*, 2004] and a scenario simulation experiment from the AOGCM atmosphere-ocean coupled model ECHAM5-MPIOM [*Roeckner*, 2005], which incorporates the effects of the Pinatubo eruption on stratospheric aerosol. Both simulations were published by *Randall et al.* [2007] and were downloaded from the CERA database (http://cera-www.dkrz.de).

[43] As it was the case for January 1990, the global long-term mean 1989–2008 of the vertical energy flux divergence (F_s − ad_{TOA}) in ERA-Interim is far from zero (+8.1 W m^{-2}), which would translate into a global cooling of 0.8 K/month (not shown). Again, this can be ascribed to the surface energy fluxes (the global 20 year mean of F_s amounts to +7.4 W m^{-2}), which reflect an overall global imbalance in the surface energy budget. *Steinheimer et al.* [2008] reported far weaker imbalances for 1 year climate runs of the then operational ECMWF forecast system; therefore, this large spin-up seems to affect mainly the short-term forecasts used here. Despite the evidence of biased absolute values of various energy budget terms like surface energy fluxes and storage rate, we see much value in analyzing their spatial and temporal variations. Since the ECMWF model version has not been changed during the two reanalyzed decades (1989–2008), the biases in ERA-Interim assimilating model should be constant in time. Jumps and inhomogeneities in fluxes and tendencies can then only arise either from abrupt changes in the observation system or from true climate fluctuations.

[44] The vertical energy flux divergence (F_s − Rad_{TOA}) was also calculated for ECHAM5 simulations and compared to ERA-Interim in Figure 7. Global mean anomalies in ERA-Interim show a jump from positive to negative values in January 1992 and a subsequent long-term decrease of approximately −4 W m^{-2}, although with a trend reversal between 2000 and 2006. Both ECHAM5 simulations indicate strong monthly variability but show no evidence of long-term variations or sudden jumps. The strongest monthly mean ERA-Interim anomalies of up to −20 W m^{-2} (which means net atmospheric warming) are detected in the eastern tropical Pacific (5°S–5°N, 150°W–90°W, not shown), in correspondence with the strong El Niño event of 1997. The response in the uncoupled ECHAM5-AMIP simulation to variability of the tropical SSTs is strong and agrees well with ERA-Interim (their correlation is 0.89 for the period 1989–1998 in the Niño-3 region). Over the same area, the coupled ECHAM5-MPIOM simulation shows different behavior (the correlations of ECHAM5-MPIOM with the uncoupled simulation and ERA-Interim are 0.06 and

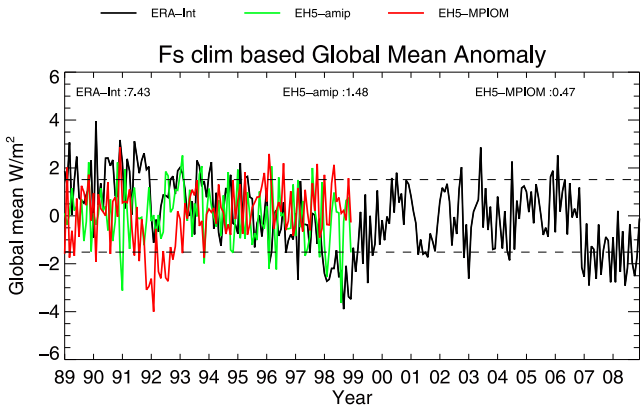

Figure 8. Time series of the global mean surface energy flux F_s anomalies and long-term mean values. The dashed line indicates the ERA-Interim standard deviation (unit is W m^{-2}).

−0.15, respectively), indicating that the signal in ERA-Interim and ECHAM5-AMIP is mostly SST driven. We argue that this perturbation of the atmospheric energy budget in ERA-Interim, which is seen only on regional scales (e.g., in the Niño-3 region), is a true climatic signal of the El Niño event. However, since (F_s − Rad_{TOA}) is an integral measure, the vertical distribution of the induced atmospheric warming cannot be studied from our diagnostics. We note that the annual means in Figure 7 should be very close to zero, since a mean of 0.1 W m^{-2} would already correspond to a global mean atmospheric warming of 0.35 K/year. Annual means of more than 1 W m^{-2} seen in Figure 7 are likely to be spurious.

[45] We performed a separate analysis of the single components (Rad_{TOA} and F_s) to explore their contribution to the interannual variability of the vertical energy flux divergence. For the TOA radiative balance, we included ISCCP-FD data into our diagnostics for the first decade (1989–1998). No evidence of long-term variability is found in all data sets. The coupled ECHAM5-MPIOM simulation and ISCCP-FD exhibit stronger monthly scale variability and, unlike ERA-Interim and ECHAM5-AMIP, also a prominent negative peak in 1991, which is related to the Pinatubo eruption. However, ISCCP-FD contains substantial biases [see *Chiodo*, 2008, Figure 6.3] and only the ocean-coupled ECHAM5-MPIOM run simulates a realistic magnitude (−4 W m^{-2}) of the total volcanic radiative forcing, a value that is in good agreement with the results of *Minnis et al.* [1993] and *Hansen et al.* [1992] and other radiation climatologies (i.e., ERBS). The volcanic TOA signal in ERA-Interim is surprisingly weak. This may be related to a conservative representation of aerosol forcing in the ERA-Interim assimilating model.

[46] F_s for ERA-Interim and the two climate model runs is shown in Figure 8. There is little variation in the TOA fluxes; accordingly, F_s resembles the temporal evolution of the net vertical energy flux divergence. The ERA-interim F_s has much larger energy fluxes into the surface (+7.4 W m^{-2} in the 20 year mean 1989–2009) than both ECHAM5 simulations (+1.5 and +0.5 W m^{-2} in the decadal mean 1989–1998, see Figure 8), and the imbalance is entirely produced over the ocean. Nevertheless, it is interesting to interpret the peaks and shifts in the ERA-Interim time series. There is a decrease (increase to the atmosphere) in ERA-Interim surface energy fluxes, with some trend reversal between 2000 and 2006, but, as for the vertical energy flux divergence, no such interannual variability is exhibited in climate models. The most evident negative peaks are found in correspondence with the Pinatubo eruption in 1991 in the coupled ECHAM5-MPIOM simulation and in late 1997 in correspondence with the warm El Niño in both ERA-Interim and ECHAM5-AMIP, which were forced with the same observed SSTs (thus suggesting that this signal is mostly SST driven). The Pinatubo negative peak in ECHAM5-MPIOM surface energy budget makes sense, since the volcanic stratospheric aerosol spread globally in the months after the eruption and led to a strong negative anomaly in the surface radiation budget because of strong scattering of solar radiation. On the other hand, the volcanic signal in ERA-Interim surface energy balance seems to be weaker, and may also be masked by a problem in data assimilation described below.

[47] F_s can be further split into turbulent and radiative surface fluxes. Figure 9 presents time series of the tropical mean (10°N–10°S) surface turbulent heat flux anomalies (LH + SH) over the oceans using ERA-Interim, HOAPS-3, and both ECHAM-5 simulations.

[48] The Pathfinder-SST AVHRR retrievals used in HOAPS-3 contain large biases in 1991–1992, resulting in an underestimation (weaker fluxes, thus the positive peak) of the latent heat flux LH and, although in minor extent, of the sensible heat flux SH (S. Bakan, personal communication, 2008).

[49] Over the eastern tropical pacific, all data sets present high correlation values with the Niño-3 index (see Table 1a). Moreover, the similarity of the correlation coefficients suggests good agreement among all data sets in the flux response to both ENSO phases in 1997–1998. The strong negative anomalies in late 1997 are SST driven and cannot be found in the coupled ECHAM5-MPIOM simulation, which of course generates its own ENSO cycles. These results indicate that the ocean acted as a heat source during warm ENSO events, inducing in this way large-scale perturbations in atmospheric energy budgets. After 1993, there is evidence of a trend toward stronger fluxes (negative anomalies mean stronger heat fluxes into the atmosphere) in

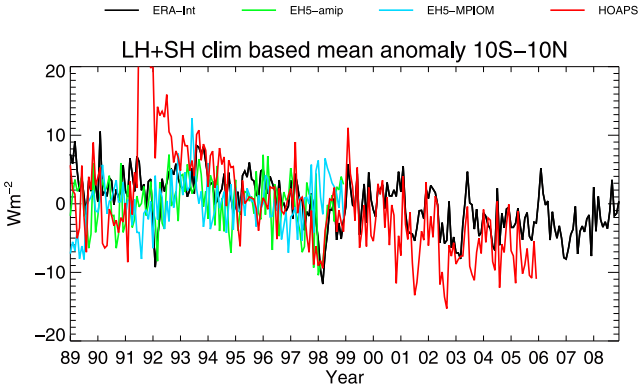

Figure 9. Time series of the tropical (10°N–10°S) surface heat flux (latent plus sensible heat flux) anomalies. Negative values indicate larger fluxes (unit is W m^{-2}).

Table 1a. Linear Trend of the Ocean Turbulent Heat Fluxes Over 1989–2005 Using Least Squares, the NAIVE Significance Test, and the Correlation With the Niño-3 Index in the Niño-3 Region[a]

LH + SH	LS Trend	Significance (%)	Niño-3 Correlation
ERA-Interim	−3.8 (−2.8)	99 (99)	0.85 (0.72)
HOAPS-v3	−12.9 (−9.5)	99 (99)	0.60 (0.28)
ECHAM5-AMIP	−0.6 (0.6)	77 (74)	0.79 (0.70)

[a]Heat fluxes are LH + SH. For ECHAM5 simulations, results are for 1989–1998. Units are W m^{-2} per 17 years for ERA+HOAPS and W m^{-2} $decade^{-1}$ for ECHAM5. Niño-3 region is 90°W–150°W, 5°N–5°S. Values in parentheses denote ENSO-removed estimates (without 1997–1998).

HOAPS-3 (−12.9 W m^{-2} over the 17 years (1989–2005) of HOAPS-3 data) and, although in minor extent (−3.8 W m^{-2} over the 20 years (1989–2008) of ERA-Interim data), in ERA-Interim. The persistence of this pattern over more than a decade lends more statistical significance to these results.

[50] The NAIVE method [*Santer et al.*, 2000] was applied to test the significance of these trends in both data sets for the surface heat (LH + SH) and energy (F_s) fluxes. Figures 10 and 11 show that the trends in HOAPS and ERA-Interim turbulent surface fluxes are significant over the subtropical oceans and agree well in magnitude over the central and eastern Pacific. Strong increases in heat fluxes are also found in the Mediterranean basin. The signal over the eastern Pacific is mostly because of ENSO sampling in both data sets since the trend pattern changes considerably over this area if the years 1997 and 1998 are excluded, and the correlations with the Niño-3 index decrease for both ERA-Interim and HOAPS-3 (see correlation values in parentheses in Table 1a). However, the global trends do not change significantly.

[51] The change in the turbulent heat fluxes produces also a negative trend in the ERA-Interim surface energy fluxes over the same areas, but no significant changes can be found in the net surface radiation Rad_S. Hence, contrary to the turbulent fluxes, the trend in the surface energy fluxes is not significant (Table 1b), since the net surface radiation balance, according to equation (3), acts as an additional noise source. The F_s time series (Figure 8) has also an interesting shift in 2006–2007 that needs further investigation. It comes mainly from the surface radiation flux time series (not shown) and coincides also with a shift in the Hovmöller diagram in Figure 13. Thus, trends in F_s must be interpreted with extreme caution.

[52] If we neglect the transports carried out by the ocean circulation, which should vanish when integrated over the whole ocean volume, and the energy flux into the ocean below 750 m, then the ocean heat storage rate is equal to F_s, averaged over the same time interval [*Zhang et al.*, 2007]. Despite the biased long-term mean of the ocean surface energy fluxes in ERA-Interim and HOAPS-3, their negative trend in turbulent heat fluxes (LH + SH) would imply a net energy loss in the global ocean. *Zhang et al.* [2007] obtained similar results for the net surface energy fluxes from the combination of ISCCP-FD surface net radiation and turbulent heat fluxes from HOAPS-2 and WHOI. Agreement is also found with *Yu and Weller* [2007], who found increasing heat fluxes during this decade from a combination of SST, satellite, and reanalysis data. However, they also show a jump in latent and sensible heat fluxes from 1991 to 1992 (Figure 6), while the SST drops from 1991 to 1992. This is in sharp contrast to the other years, where heat fluxes and SSTs are positively correlated. Our

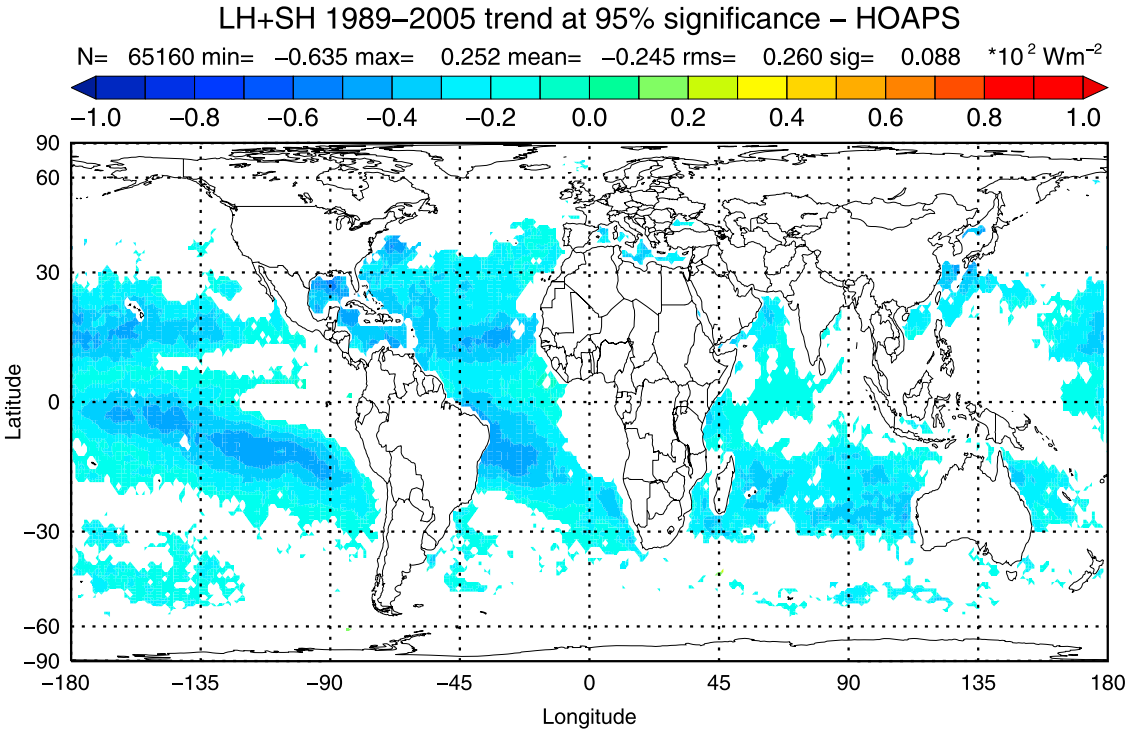

Figure 10. Regions with statistically significant (at 95%) decadal (1989–2005) trend of HOAPS-3 surface heat fluxes (latent plus sensible heat) (unit is W m^{-2} $decade^{-1}$).

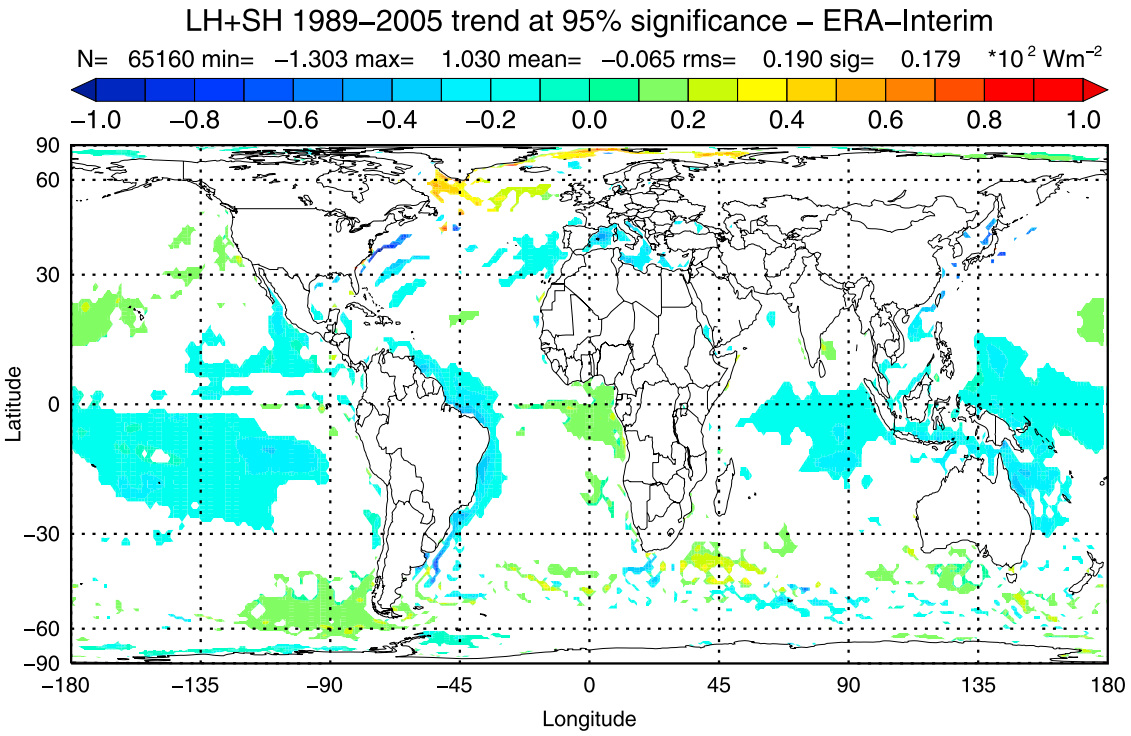

Figure 11. Regions with statistically significant (at 95%) decadal (1989–2005) trend of ERA-Interim surface heat fluxes (unit is W m^{-2} $decade^{-1}$).

analysis and the lack of correlation with an SST jump let us suspect that this jump in their data is artificial and may have led to an overestimation of the heat flux trends in their paper.

[53] In ERA-Interim and HOAPS, either (1) an increase in the assimilating model wind speed, (2) an increase in the low tropospheric temperature, and/or (3) a decrease in the relative humidity can explain the occurrence of this long-term variation in the heat fluxes. However, we note a lack of consistency among various sources of evidence regarding this trend pattern. First, the uncoupled ECHAM5 simulation, which is constrained with observed SSTs, does not exhibit this trend. Second, direct oceanic measurements [e.g., *Levitus et al.*, 2000; *Willis et al.*, 2004] rather hint at a net warming, which would imply net heat fluxes into the oceans. Third, the anomalies in the vertical energy flux divergence (Figure 7) are too large, since an annual average of 1 W m^{-2} would imply a global warming of the atmosphere to the order of 3.5 K/yr. Further research is needed to assess to what extent this trend is a result of biased SSM/I measurements in ERA-Interim and HOAPS-3 or natural variability (or both).

[54] In section 4, our focus was on the vertically integrated horizontal energy divergence, applying all corrections and methods discussed in section 4. However, when looking at time series, this quantity shows little variation in zonal belt means. The only interesting feature is a pronounced positive anomaly in late 1997 over the tropics, which is indicative of an anomalous energy export by the atmosphere over the region with the strongest warming response to the El Niño (not shown).

[55] On the other hand, the temporal evolution of the forecast atmospheric storage rate (shown as a Hovmöller diagram in Figure 12) captured our attention. The very high variability in middle and high latitudes is correlated to surface pressure anomalies, while in the tropics, where the annual cycle is weak, a preferred sign of the tendencies indicates an imbalance between the climate of the assimilating model and the analyzed model state. The maximum of 6 W m^{-2} in 1991 is related to the Pinatubo eruption, which caused heating rates of 0.25 K/d in the stratosphere [*Andersen et al.*, 2001], but the most interesting feature is the jump from positive to negative anomalies a few months later. The shift before and after January 1992 indicates an imbalance between the climate of the assimilating model (12 h model forecasts) and the analyzed model state (analysis). Prior to 1992, two bad channels on DMSP-8 were blacklisted, which significantly affected the humidity information over the tropical oceans. After 1992, new SSM/I clear-sky radiances had been made available on DMSP-10 (D. Dee, personal communication, 2008). In this way, the analyzed climate state is energetically too low before 1992, and the model tends to converge toward its own energetically higher climate, producing systematic positive anomalies in the energy tendency (which, if vertically integrated, is the atmospheric storage rate).

[56] We calculated 12 h analysis increments as defined in equation (10) of the atmospheric storage rate (shown as a

Table 1b. Same as Table 1a but for the Surface Energy Fluxes (F_s)[a]

F_s	LS Trend	Significance (%)
ERA-Interim	−4.0 (−3.1)	93 (79)
ECHAM5-AMIP	−0.5 (0.0)	57 (50)
ECHAM5-MPIOM	+1.3 (1.5)	70 (66)

[a]Values in parentheses denote ENSO-removed estimates (without 1997–1998).

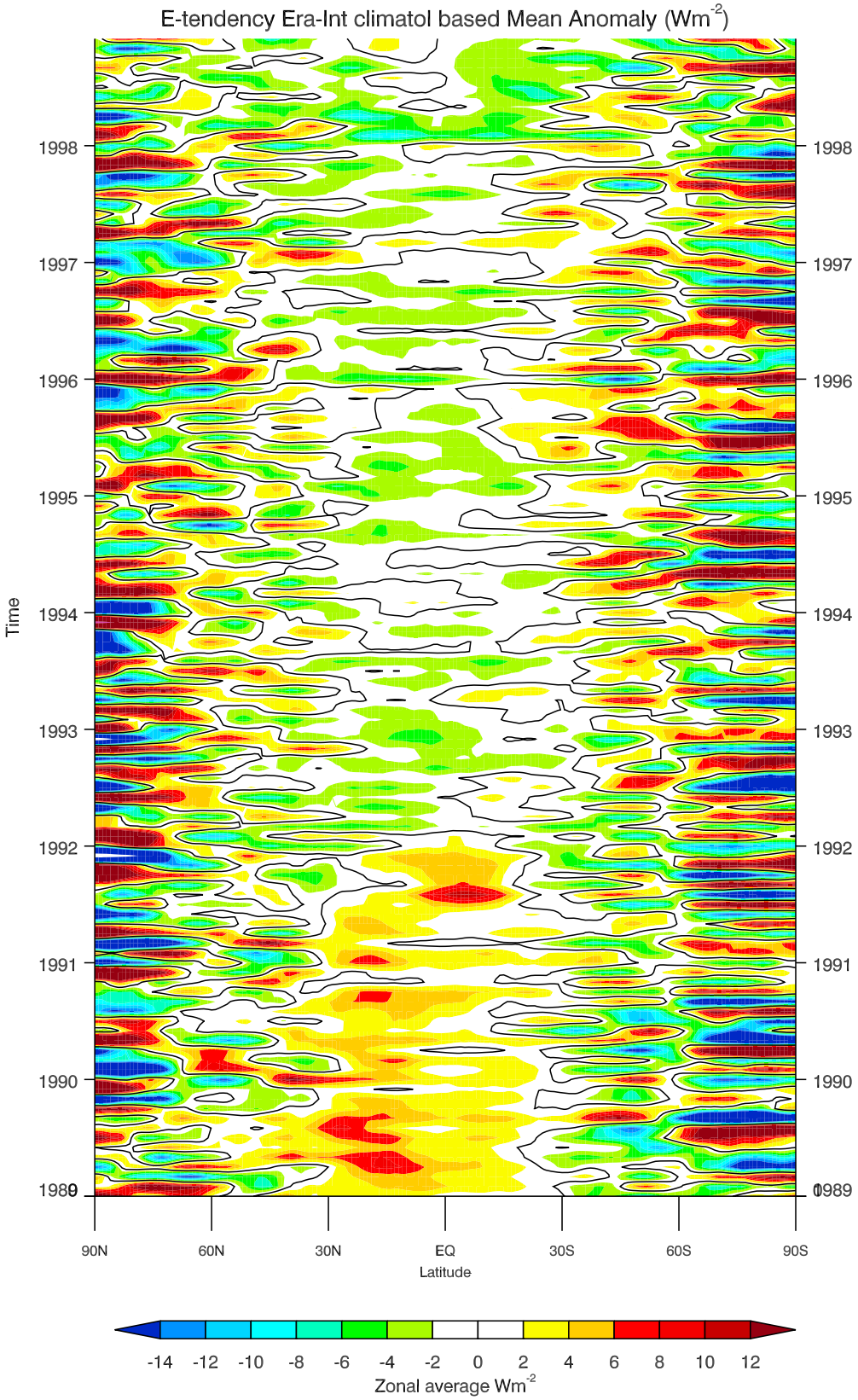

Figure 12. Hovmöller plot of atmospheric rate of storage ($\partial\langle e\rangle/\partial t$) zonal mean anomalies in ERA-Interim (in W m^{-2}, 1 W m^{-2} is equivalent to a vertical mean tendency of 0.01 K d^{-1}).

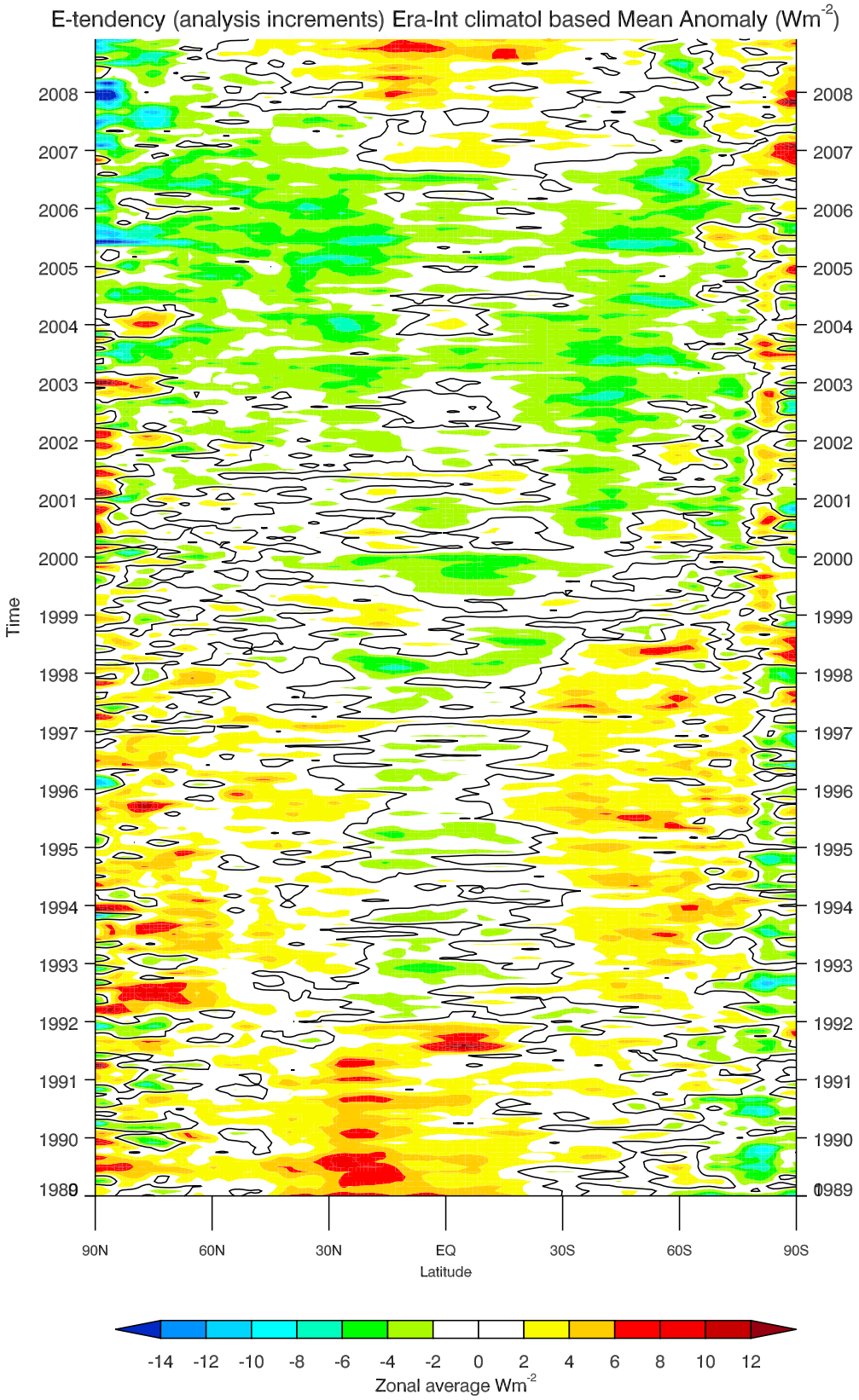

Figure 13. Hovmöller plot of ERA-Interim corrected 12-h analysis increments of storage rate, calculated as in equation (10) (unit is W m^{-2}).

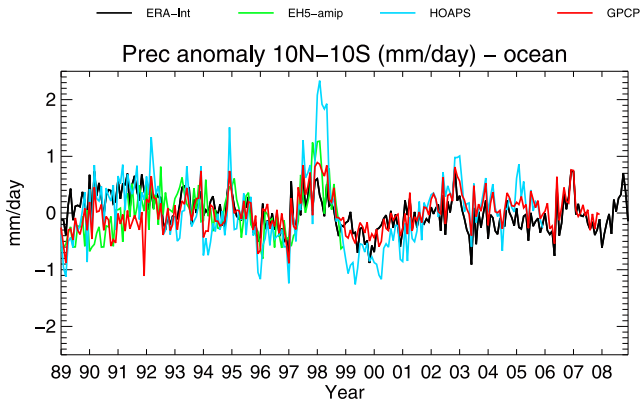

Figure 14. Tropical precipitation anomaly over the ocean (10°N–10°S) (unit is mm d^{-1}).

Hovmöller plot in Figure 13) and extended the diagnostics to 2008. The analysis increments are by definition the difference between analysis and background forecast. Hence, they account for the influence of the observational system in the assimilation cycle. The usual definition of analysis increment of total energy would be the difference between the total energy content in analysis and forecasts (with units J m^{-2}), but we converted it into a tendency by applying a time derivative, obtaining in this way the same units of the atmospheric storage rate (W m^{-2}). In the work by *Andersen et al.* [2001], the use of analysis increments was similar, but here we use 12 h increments instead of 24 h. This time resolution maximizes their utility to detect model imbalances, since 12 h is the cycle in the 4D-variational assimilation used in ERA-Interim. The shift in 1992 is replicated in both storage rate and precipitable water tendency (although with different sign), thus confirming its artificial nature (Figures 13–19). Another shift in late 2006 in Figure 13 corresponds well to a shift observed in the F_s time series in Figure 8. The analysis increments of the atmospheric storage rate contain less noise in the extra-tropics than the original field (Figure 12) but still show climatic signals as the strong warming in late 1991 induced by the Pinatubo's volcanic aerosol in the stratosphere. The peak in the analysis increments in late 1991 shows that there is strong imbalance between the climate of the assimilating model in ERA-Interim and the assimilated state. This is an indication either that the radiation perturbation through the aerosol is not well represented in the assimilating model of ERA-Interim or that the aerosol signal in the satellite radiances is misinterpreted as temperature or moisture signal. We found that the perturbation of the TOA net radiation in ERA-Interim is rather weak [*Chiodo*, 2008, Figure 6.3] compared with climate models with volcanic forcing. This inconsistency implies, as in ERA-15 [*Andersen et al.*, 2001], that the transient atmospheric forcing related to the volcanic eruption is present in ERA-Interim, but the representation of volcanic aerosol in the assimilating model is too weak. *Dee and Uppala* [2008], who analyzed this period in much detail, also argue that the former reason is the principal cause for this imbalance.

[57] We conclude our long-term diagnostics by exploring the decadal changes of the global water budget. The interannual variability of the freshwater flux (*P-E*) is mostly dominated by the precipitation, especially in the tropics. Thus, climatic fluctuations in the tropical precipitation are of special interest. The tropical ocean precipitation anomaly time series is presented in Figure 14. Besides substantial differences in the absolute precipitation values, all data sets present similar variability in the first decade (the correlations range from 0.36 for ECHAM5-ERA to 0.80 for HOAPS-GPCP). Interestingly, the agreement between HOAPS-3 and ERA-Interim is worse in the second decade (1998–2005) than in the first (1989–1998). All data sets contain a positive peak in 1997–1998, which is related to ENSO. No obvious artificial shifts are found in HOAPS-3, GPCP-2, and ERA-Interim; therefore, their interannual variability should be at least in part related to true climate signals. It should be reminded that GPCP-2 rain estimates are more uncertain over the ocean than over land, but we plot them for illustrative purposes. They correlate well with both ERA-Interim (0.57) and HOAPS-3 (0.80), which is quite obvious, since they use the same satellite retrievals. HOAPS-3 anomalies are larger than in ERA-Interim, GPCP-2, and ECHAM5 simulations, which is indicative of stronger seasonal fluctuations in ITCZ intensity and position but may also be caused by noise in the retrieval algorithm. Warm ENSO events are correlated with large positive precipitation anomalies in the eastern and central Pacific that also stand out in zonal average with anomalies of up to 1.5 mm d^{-1}. During cold ENSO (La Niña in 1989 and 1998) events, the tropical precipitation shows the opposite patterns. Although the same microwave satellite product (SSM/I) is used in ERA-Interim, GPCP-2, and HOAPS-3, and the same SSTs drive reanalysis and the uncoupled ECHAM5 simulation, the precipitation variations from HOAPS-3 seem excessive. In the past decade (1999–2008), both HOAPS-3 and ERA-Interim show no clear trends and jumps.

[58] A similar interannual variability plot is also shown in Figure 15 for the tropical land precipitation. ENSO-related anomalies in the ITCZ are generally of opposite sign to those over the ocean. Warm ENSO events produce droughts in Indonesia and weaker monsoon rains in India, along with anomalous precipitations in the Andes region, a pattern which stands out as a large negative tropical precipitation anomaly in the zonal mean. Taking GPCP-2 as a validation baseline for its high quality over land, the agreement (although with some phase shift of a few months and

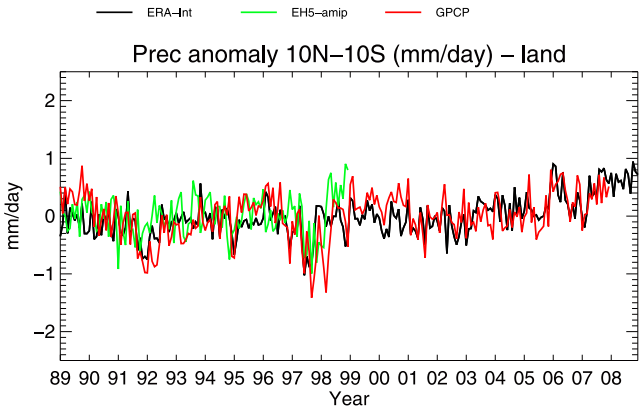

Figure 15. Tropical precipitation anomaly over land (10°N–10°S) (unit is mm d^{-1}).

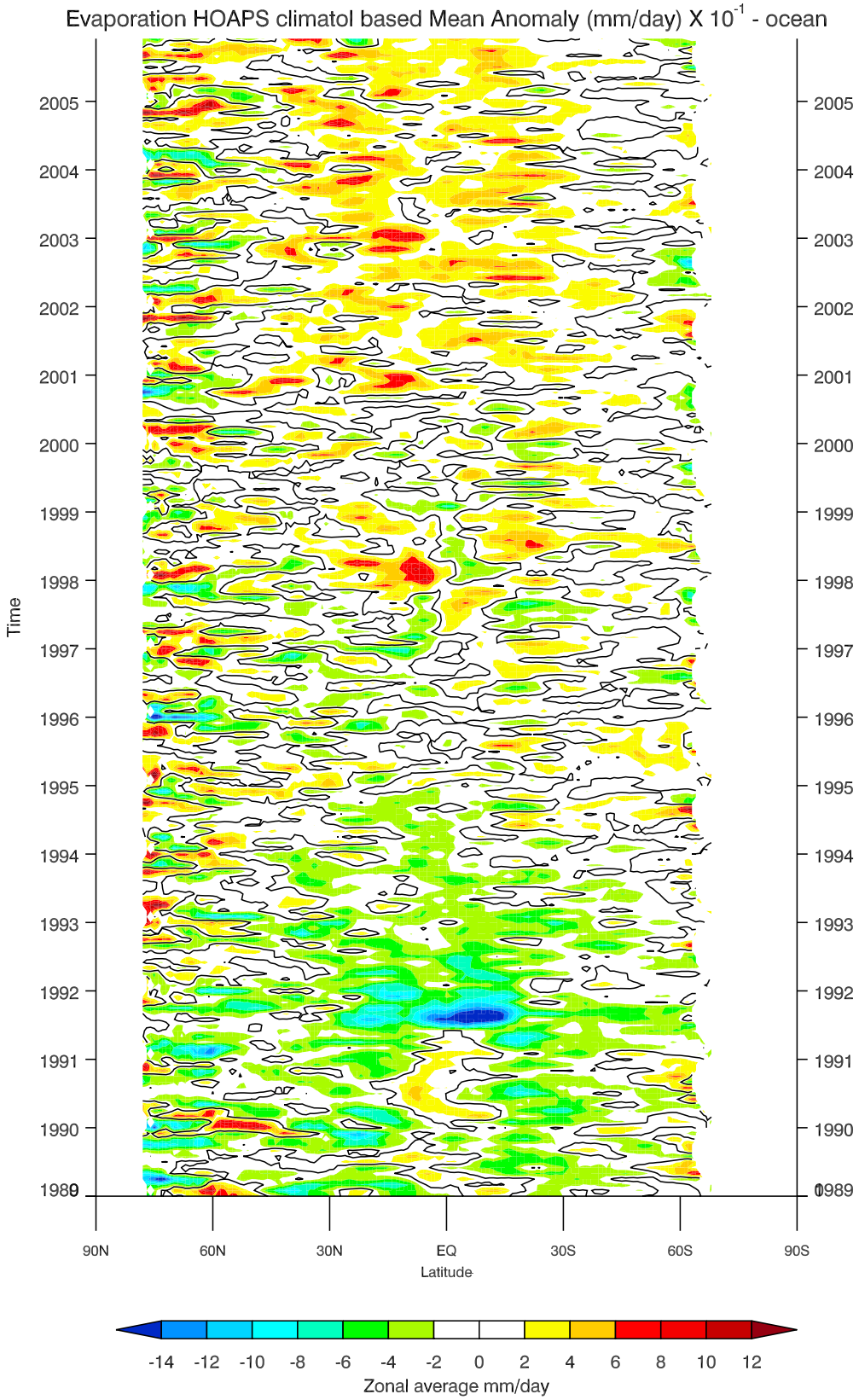

Figure 16. Hovmöller plot of the HOAPS-3 evaporation zonal mean anomalies over the ocean (unit is 10^{-1} mm d^{-1}).

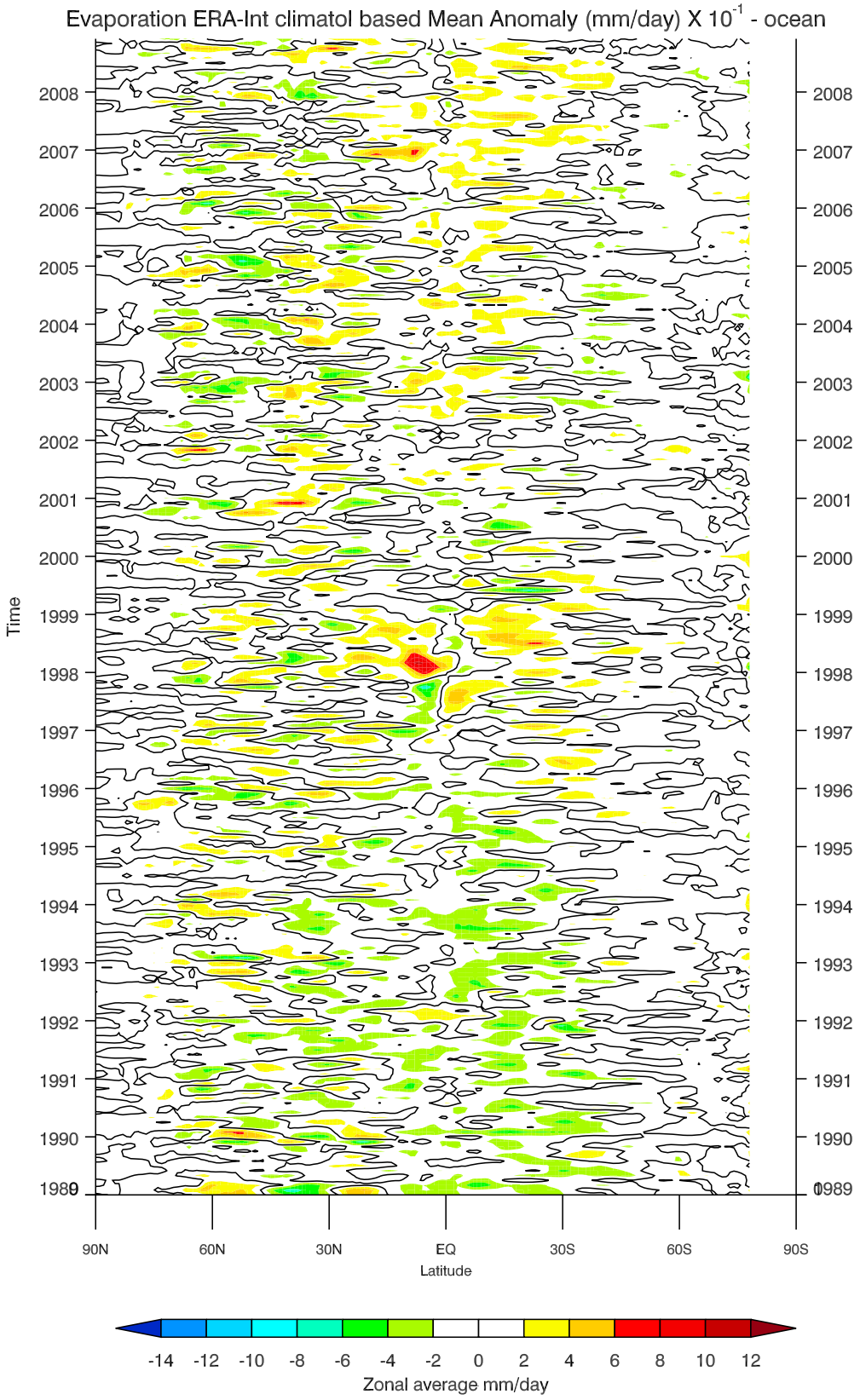

Figure 17. Same as Figure 16 but from ERA-Interim (unit is 10^{-1} mm d^{-1}).

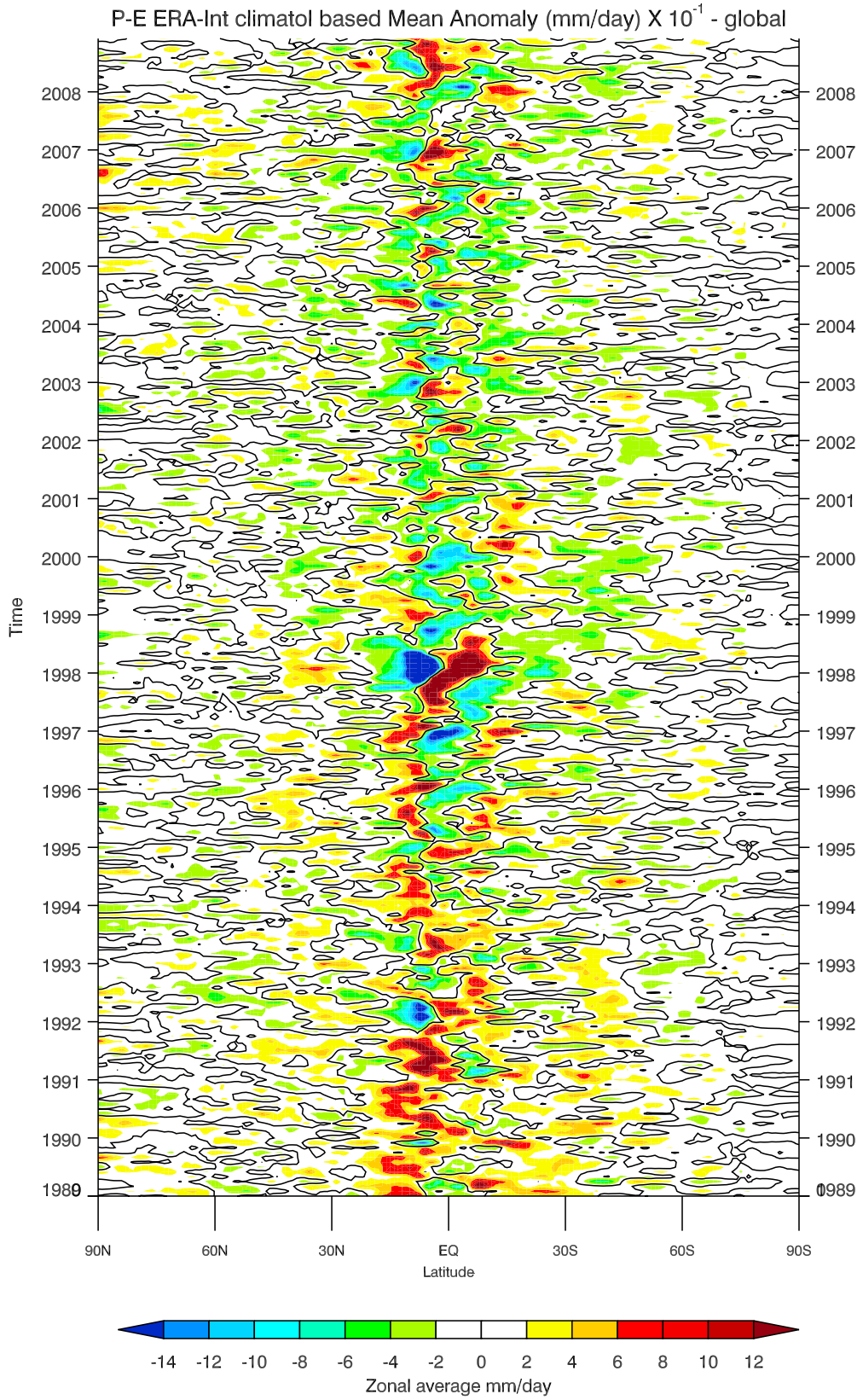

Figure 18. Hovmöller plot of ERA-Interim global freshwater flux (*P-E*) zonal mean anomalies (unit is 10^{-1} mm d^{-1}).

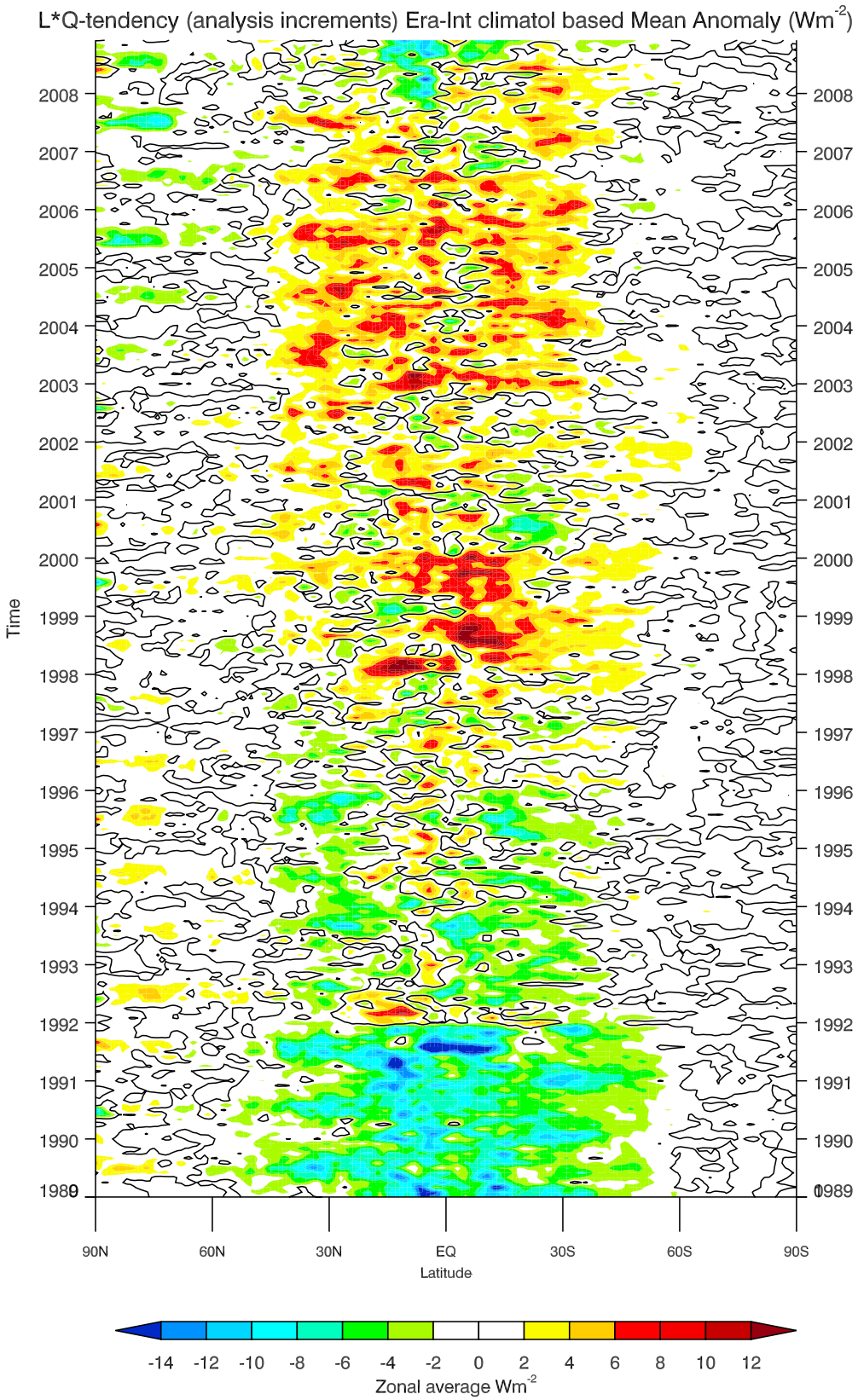

Figure 19. Hovmöller plot of ERA-Interim 12 h analysis increments of precipitable water tendency ($\partial w/\partial t$) zonal mean anomalies. Fields have been multiplied with latent heat L to obtain W m^{-2} units.

quantitative discrepancy) in 1997–1998 indicates that ERA-Interim and ECHAM5 capture the land precipitation response in the winter season to ENSO. The errors in the phase and amplitude of the variations in the uncoupled ECHAM5-AMIP simulation may be related to the model failure in reproducing the observed negative precipitation response in the Indian monsoon and Australia, because of the constraint imposed by prescribed SSTs [*Hagemann et al.*, 2006]. Another remarkable feature is the steady increase in land precipitation from 2000 until present, which accounts to approximately 1 mm d^{-1}. Since it is present in both ERA-Interim and GPCP-2 this change appears to be a robust feature.

[59] To better understand the turbulent surface flux trends in Figures 9–11 we also show Hovmöller plots of ERA-Interim and HOAPS evaporation. Strong anomalies in evaporation in correspondence with El Niño in 1997 can be found not only in tropical but also in subtropical regions of the Southern Hemisphere (Figures 16–17), which is a true signal of abrupt changes in tropical atmospheric circulation patterns associated with ENSO. In HOAPS-3, the strong peak in evaporation shortly after the Pinatubo eruption (1991) is mostly spurious and could be related (1) to the previously described problems in the Pathfinder-SST retrievals, which affected the ocean heat fluxes, and (2) to the SSM/I platform change that was responsible for the shift in the tropical rate of storage computed with ERA-Interim data. It is interesting to note that HOAPS-3 evaporation shows strong positive trends from 1998 over wide parts of the globe, in agreement with NCEP reanalysis for this period [*Trenberth and Guillemot*, 1995]. The anomalies, particularly in low latitudes, amount in some months between 2000 and 2005 to 1 mm d^{-1}. ERA-Interim (Figure 17) shows a much weaker trend than HOAPS, and it is confined to the subtropical portion of the Southern Hemisphere during the past 5 years of the time series. The increase in ocean evaporation and the coincident increase in land precipitation (Figure 15) of the same magnitude (1 mm d^{-1}) is indicative of stronger inland moisture fluxes in ERA-Interim, possibly mandated by an acceleration in the Hadley circulation. However, further research is needed to investigate the dynamical aspects of this pattern in the tropical hydrological cycle.

[60] Another interesting signal is the increase in HOAPS-3 ocean precipitation at approximately 5°N during the past 5–6 years (1999–2005), which was also apparent in Figure 14. It may be indicative of an intensification of the ITCZ. However, we lend more credibility to long-term changes in the ERA-Interim moisture budgets than in HOAPS-3, since HOAPS-3 fluxes are corrupted from biases in SSM/I retrievals (e.g., at the time of the Pinatubo eruption). ERA-Interim values are more homogenous in time and present good correlation with GPCP-2 (the correlation value in land precipitation is 0.65).

[61] The Hovmöller plot of the freshwater flux (*P*-*E*) from ERA-Interim (Figure 18) shows strong interannual variations (e.g., ENSO). Global mean trends of *P*-*E* would be unphysical, since an increase/decrease would imply net global drying/moistening of the atmosphere. Although the Hovmöller plot does not give any evidence of large long-term changes of this quantity (which accredits the good quality of ERA-Interim data), we see some predominance of weak negative anomalies in low latitudes during the period 2000–2007 (thus indicative of a slight negative trend) and of positive anomalies during the first reanalyzed years which seem suspicious.

[62] We therefore calculated the analysis increments of the precipitable water tendency in a similar fashion as for the atmospheric storage (see equation (10) and Figure 13). This quantity (Figure 19) shows a clear positive trend, and the strongest signals are in correspondence with the Pinatubo eruption and El Niño in late 1997. Positive moisture increments imply that the model is systematically introducing more moisture to the new assimilated observations, thus resulting in negative anomalies in freshwater flux anomalies (*P*-*E*). We note that there is indeed such anticorrelation in low latitudes (see Figure 18); that is, the positive freshwater anomalies during the first years agree with the negative anomalies in the moisture increments, and the weak negative trend in freshwater flux during the period 2000–2007 coincide with positive anomalies over the same latitudes in the increments. This coupled variability proves the internal consistency of our ERA-Interim moisture diagnostics, since the analysis increments and the vertical fluxes (*E* and *P*) are calculated from completely different fields. The moisture balance is closer to zero than in ERA-40, which is the result of improved moisture analysis and model physics in ERA-Interim [*Uppala et al.*, 2008]. However, the shifts in the analysis increments also indicate that the apparent slight negative trend from 2000 to 2007 in *P*-*E* is very likely spurious.

[63] As a consequence, we must say that data inconsistencies in HOAPS and to a lesser extent ERA-Interim still limit our ability to investigate interannual variability or even trends of surface moisture and energy budgets. The previously mentioned analysis shows, however, that additional diagnostics from reanalyses, especially analysis increments, provide valuable information for the interpretation of surface flux variations.

6. Conclusions

[64] Surface fluxes and analyses from ERA-Interim comprise a valuable new data set for assessing monthly mean regional budgets as well as 20 year time series of budget quantities. In the first part of this paper, we present methods how to take full advantage of the fields provided by ERA-Interim. In particular, we discussed methods for estimating the horizontal energy and moisture divergence. It was shown that direct estimates from analysis contain noise due to mass imbalances as well as due to the time discretization errors. We presented an alternative way to calculate horizontal divergences, namely, to determine them from the difference between vertically integrated tendencies and vertical fluxes. We developed corrections of mass imbalances in surface pressure tendencies and spin-up effects in vertical energy fluxes and demonstrated that better horizontal transport divergences can be inferred with this method than available in the literature.

[65] While the horizontal flux divergences are important for regional budgets, they must be zero in the global mean and, therefore, cannot indicate climate changes in the global mean energy budget. These can be seen only in the vertical fluxes. The time evolution of these has been analyzed, and

ERA-Interim has been compared with other data sources. The task of investigating interannual variations in global budgets is complicated by homogeneity issues. An important goal of our analysis was to detect changes and discriminate the artificial shifts from those related to real climatic perturbations.

[66] There is evidence of a trend during the period 1992–2008 in the ERA-Interim turbulent surface heat fluxes, which is found to be highly significant over wide parts of the subtropical Pacific and in agreement with HOAPS-3. However, there is contrasting evidence from models (ECHAM5 simulation constrained with observed SSTs) and direct oceanic observations, and the trend in the surface energy fluxes is not significant.

[67] Our analysis also showed that the most evident tropical and global variations of the surface energy fluxes and of the freshwater flux are related to ENSO. The 1997 El Niño was associated with enhanced oceanic evaporation, surface heat fluxes, anomalous precipitation patterns, and energy export from the Niño region. All data sets (ERA-Interim, HOAPS, and ECHAM5) agree qualitatively in the ENSO-related precipitation changes over the oceans, although quantitative discrepancies exist. We found indications of trends of the tropical hydrological cycle in ERA-Interim and especially HOAPS-3 over the 20 year period; however, they seem questionable especially in HOAPS. Among all these changes, only the recent (2000–2008) increase in tropical land precipitation is likely to be robust and needs further investigation.

[68] The employment of 12 h analysis increments enabled us not only to detect artificial breaks in ERA-Interim but also to certify internal consistency of energy and moisture budgets because of their agreement in interannual variability with vertical fluxes. There was a change in the assimilation of SSM/I data in January 1992, which produced a shift in the ERA-Interim tropical atmospheric storage rate and precipitable water tendency. A similar pattern was also found in 2007. Also, the global mean surface energy flux is too large in ERA-Interim, indicating that model spin-up still affects vertical energy fluxes.

[69] Despite the problems in the surface fluxes no artificial breaks could be detected in assimilated state quantitites, suggesting that a great step toward better temporal homogeneity has been taken through the production of ERA-Interim.

[70] To conclude, some issues still need to be regarded in future reanalyses. A further reduction of spin-up effects and imbalances in the assimilation cycle is needed to achieve a balance in the surface energy budget if diagnostic evaluations are carried out with 12 h model integration. Our results also suggest that the vertically integrated horizontal flux divergences should be stored routinely during the forecast runs of the assimilating model, avoiding large time sampling errors in budget terms that can be only calculated directly. When reanalysis data are used in climatic studies, these issues need accurate treatment, e.g., by implementing the corrections and using the methods proposed in this paper. Special attention should be awarded to inhomogeneities, which stem from changes in the observing system and hence are not related to true climate signals.

[71] **Acknowledgments.** The authors gratefully acknowledge Martin Steinheimer for his extensive comments and discussions. Special thanks also to ECMWF for providing ERA-Interim data. Paul Berrisford also helped in clarifying the manuscript; D. Dee (ECMWF), S. Bakan (MPI-M), and Y.-C. Zhang (GISS-NY) gave comments and personal communications. This work was supported by P18120-N10 of the Austrian Science Funds, by the ECMWF special project "Homogenization of the global radiosonde temperature and wind data set," and by the Spanish Project Consolider "Supercomputing and e-science" CSD2007-00050-II-PR4/07.

References

Adler, R. F., et al. (2003), The version-2 Global Precipitation Climatology Project (GPCP) monthly precipitation analysis (1979-present), *J. Hyrdrometeorol.*, *4*, 1147–11,167.

Andersen, U. J., E. Kaas, and P. Alpert (2001), Using analysis increments to estimate atmospheric heating rates following volcanic eruptions, *Geophys. Res. Lett.*, *28*(6), 991–994.

Chiodo, G. (2008), Decadal changes in the global energy and water budgets, Diploma thesis, 94 pp., Univ. of Vienna, Vienna. (Available at http://www.univie.ac.at/IMG-Wien/dipldiss/dipl/DA_Chiodo.pdf)

Climate Change Science Program (2006), Temperature trends in the lower atmosphere: Steps for understanding and reconciling differences, report, Washington, D. C.

Dee, D., and S. Uppala (2008), Variational bias correction in ERA-Interim, *Tech. Memo., 575*, 26 pp., Eur. Cent. for Med.-Range Weather Forecasts, Reading, U. K. (Available at http://www.ecmwf.int/publications/library/ecpublications/_pdf/tm/501-600/tm575.pdf)

European Centre for Medium-Range Weather Forecasts (2007), *IFS documentation—Cy31r1, operational implementation of Cy31r1. Part IV: Physical processes*, Reading, U. K. (Available at http://www.ecmwf.int/research/ifsdocs/CY31r1/index.html)

Hagemann, S., K. Arpe, and E. Roeckner (2006), Evaluation of the hydrological cycle in the ECHAM5 model, *J. Clim.*, *24*, 3810–3827.

Haimberger, L. (2006), Towards temporally homogeneous evaluations of the observed global atmospheric circulation, habilitation thesis, 153 pp., Univ. of Vienna, Vienna. (Available at http://homepage.univie.ac.at/leopold.haimberger/raobcore1-Dateien/Habilschrift_full.pdf)

Haimberger, L., B. Ahrens, F. Hamelbeck, and M. Hantel (2001), Impact of time sampling on atmospheric energy budget residuals, *Meteorol. Atmos. Phys.*, *77*, 167–184.

Hansen, J., A. Lacis, R. Ruedy, and M. Sato (1992), Potential climate impact of mount Pinatubo eruption, *Geophys. Res. Lett.*, *19*(2), 215–218.

Hantel, M. (2005), *Observed Global Climate, Landolt-Brnstein: Numer. Data and Funct. Relat. in Sci. and Technol.-New Ser.*, group 5, *Geophysics*, vol. 6, 567 pp., Springer, Berlin.

Jost, V., S. Bakan, and K. Fennig (2002), HOAPS—A new satellite-derived freshwater flux climatology, *Meteorol. Z.*, *11*(1), 61–70.

Levitus, S., J. I. Antonov, T. P. Boyer, and C. Stephens (2000), Warming the world ocean, *Science*, *287*, 2225–2229.

Minnis, P., E. F. Harrison, L. L. Stowe, G. G. Gibson, F. M. Denn, D. R. Doelling, and W. L. Smith Jr. (1993), Radiative climate forcing by the Mount Pinatubo eruption, *Science*, *259*, 1411–1415.

Peixoto, J. P., and A. H. Oort (1992), *Physics of Climate*, 520 pp., Am. Inst. of Phys., College Park, Md.

Randall, D. A., et al. (2007), Climate models and their evaluation, in *Climate Change 2007: The Physical Science Basis—Contribution of Working Group I to the Fourth Assessment Report of the Intergovernmental Panel on Climate Change [electronic]*, edited by S. Solomon et al., chap. 8, Cambridge Univ. Press, Cambridge, U. K.

Roeckner, E. (2004), EH5-T63L31-AMIP run no.1, monthly mean values, http://cera-www.dkrz.de, Clim. and Environ. Retrieval and Arch. Database, World Data Cent. for Clim., Hamburg, Germany.

Roeckner, E. (2005), IPCC MPI-ECHAM5-T63L31 MPI-OM-GR1.5L40 20C3M-all run no.1: Atmosphere monthly mean values, http://cera-www.dkrz.de, Clim. and Environ. Retrieval and Arch. Database, World Data Cent. for Clim., Hamburg, Germany.

Roeckner, E., et al. (2003), The atmospheric general circulation model ECHAM5—Part 1: Model description, *Rep. 349*, 129 pp., Max-Planck Inst. für Meteorol., Hamburg, Germany.

Santer, B. D., T. M. L. Wigley, J. S. Boyle, D. J. Gaffen, J. J. Hnilo, D. Nychka, D. E. Parker, and K. E. Taylor (2000), Statistical significance of trends and trend differences in layer-average atmospheric temperature time series, *J. Geophys. Res.*, *105*(D6), 7337–7356.

Simmons, A., S. Uppala, D. Dee, and S. Kobayashi (2006), ERA-Interim: New ECMWF reanalysis products from 1989 onwards, *ECMWF Newsl.*, *110*, 25–35.

Steinheimer, M., M. Hantel, and P. Bechtold (2008), Convection in Lorenz's global energy cycle with the ECMWF model, *Tellus, Ser. A*, *60*(5), 1001–1022.

Trenberth, K. E. (1991), Conservation of mass in ECMWF analysis, *J. Clim.*, *4*, 707–722.
Trenberth, K. E. (1997), Using atmospheric budgets as a constraint on surface fluxes, *J. Clim.*, *10*, 2796–2809.
Trenberth, K. E., and J. M. Caron (2001), Estimates of meridional atmosphere and ocean heat transports, *J. Clim.*, *14*, 3433–3443.
Trenberth, K. E., and C. J. Guillemot (1995), Evaluation of the global atmospheric moisture budget as seen from analysis, *J. Clim.*, *14*, 2255–2272.
Trenberth, K. E., and L. Smith (2009), The three dimensional structure of the atmospheric energy budget: Methodology and evaluation, *Clim. Dyn.*, *32*(7–8), 1065–1079, doi:10.1007/s00382-008-0389-3.
Trenberth, K. E., and D. P. Stepaniak (2004), The flow of energy through the Earth's climate system, *Q. J. R. Meteorol. Soc.*, *100*, 2677–2701.
Trenberth, K. E., J. M. Caron, and D. P. Stepaniak (2001), The atmospheric energy budget and implications for surface fluxes and ocean heat transports, *Clim. Dyn.*, *17*, 259–276.
Trenberth, K. E., D. P. Stepaniak, and J. M. Caron (2002a), Accuracy of atmospheric energy budgets, *J. Clim.*, *15*, 3343–3360.
Trenberth, K. E., D. P. Stepaniak, and J. M. Caron (2002b), Interannual variations in the atmospheric heat budget, *J. Geophys. Res.*, *107*(D8), 4066, doi:10.1029/2000JD000297.
Uppala, S. M., et al. (2005), The ERA-40 re-analysis, *Q. J. R. Meteorol. Soc.*, *131*, 2961–3012.
Uppala, S. M., D. Dee, S. Kobayashi, P. Berrisford, and A. Simmons (2008), Towards a climate data assimilation system: Status update of ERA-Interim, *ECMWF Newsl.*, *115*, 12–18.
Willis, J. K., D. Roemmich, and B. Cornuelle (2004), Interannual variability in upper ocean heat content, temperature, and thermosteric expansion on global scales, *J. Geophys. Res.*, *109*, C12036, doi:10.1029/2003JC002260.
Yu, L. S., and R. A. Weller (2007), Objectively analyzed air-sea heat fluxes for the global ice-free oceans (1981–2005), *Bull. Am. Meteorol. Soc.*, *88*, 527–539.
Yu, R., M. Zhang, and R. D. Cess (1999), Analysis of the atmospheric energy budget: A consistency study of available data sets, *J. Geophys. Res.*, *104*, 9655–9661.
Zhang, Y.-C., and W. B. Rossow (1997), Estimating meridional energy transports by the atmospheric and oceanic general circulations using boundary fluxes, *J. Clim.*, *10*, 2358–2372.
Zhang, Y.-C., A. A. Lacis, V. Oinas, and M. I. Mishchenko (2004), Calculation of radiative fluxes from the surface to top-of atmosphere based on ISCCP and other global data sets: Refinements of the radiative transfer model and the input data, *J. Geophys. Res.*, *109*, D19105, doi:10.1029/2003JD004457.
Zhang, Y.-C., W. B. Rossow, J. P. Stackhouse, A. Romanou, and A. B. Wielicki (2007), Decadal variations of global energy and ocean heat budget and meridional energy transports inferred from recent global data sets, *J. Geophys. Res.*, *112*, D22101, doi:10.1029/2007JD008435.

G. Chiodo, Departamento de Fisica de la Tierra, Astronomia y Astrofisica II, Facultad de Ciencias Fisicas, Universidad Complutense de Madrid, Ciudad Universitaria, E-28040 Madrid, Spain. (gchiodo@fis.ucm.es)
L. Haimberger, Department for Meteorology and Geophysics, University of Vienna, A-1090 Vienna, Austria.